Segmental Orientation in Uniaxially Deformed Polymer Networks and Application to Orientation-Induced Crystallization

Masaru Matsuo,*,† Yuri Sugiura,† Tsunehisa Kimura,‡ and Tetsuya Ogita§

Department of Textile and Apparel Science, Faculty of Human Life Environment, Nara Women's University, Nara 630-8263, Japan; Department of Industrial Chemistry, Faculty of Engineering, Tokyo Metropolitan University, Hachiooji 192-03, Japan; and Department of Material Science and Engineering, Yamagata University, Yonezawa 992, Japan

Received May 5, 2000; Revised Manuscript Received March 8, 2002

ABSTRACT: An orientational distribution function is employed for the first time to describe segmental orientation in a uniaxially deformed network. The model assumes that each chain expands between two active junctions that displace affinely with the macroscopic deformation. The model was first introduced by Erman et al. and used to evaluate the second-order Legendre polynomial of the segment orientation. This paper extends their model to compute the orientation factors of a single segment up to the eighth order, thereby enabling a more complete description of the orientational distribution to be estimated. As an application of these results to oriented crystallization of polymeric systems, an evaluation of the orientational distribution function for crystallites in a polyethylene film manufactured by a calendering method is presented. The resulting theoretical distribution of the crystallites is in good agreement with the experimental function measured by X-ray diffraction techniques. Furthermore, the small-angle light-scattering pattern under H_v polarization was estimated by assuming a rod to be an aggregation of cylindrical clusters oriented with a kinetically determined distribution. The calculated light-scattering patterns are also in good agreement with the observed ones.

Introduction

Polymer molecules are intrinsically anisotropic in structure. This causes anisotropy in bulk mechanical and optical properties. The contribution of individual polymeric structural units to the bulk properties can be represented in terms of the anisotropy of the units and their orientation. To estimate structural anisotropy in a bulk sample, a mathematical representation of the orientation distribution of the structural units and the reciprocal lattice vectors within the units was first presented many years ago in terms of a series of generalized spherical harmonics by Roe and Krigbaum.[1−3] Although their geometrical treatment is powerful, it neglects the statistical aspect of the molecular chains.[3] To incorporate this aspect, the segmental orientation in uniaxially deformed elastic networks has been discussed both in terms of gaslike theories[4,5] where the effects of intermolecular interferences between chain segments are neglected as well as in terms of liquidlike theories[6−8] where the intermolecular forces leading to orientation-dependent packing entropy are considered.

Recently, Erman et al. proposed a new liquidlike theory which includes the effect of chain stiffness.[9,10] They formulated the segmental orientation in the deformed network in terms of the second-order Legendre polynomial. At large values of the length-to-width ratio of a structural unit of a chain, however, the calculated second-order orientation factor showed a positive residual value even in the undrawn state ($\lambda = 1$), although the value must be zero due to the random orientation in the undeformed state. To avoid this contradiction, Matsuo et al. proposed a modified lattice model[11] and was able to avoid the contradictory result of the liquid model at ($\lambda = 1$).

For the gaslike theories,[4,5] another important analysis of segmental orientation in uniaxially deformed networks was also proposed by Erman et al.[12] Following the general formulation of the segmental orientation of real unoriented chains initiated by Nagai[13] and Flory,[14] which entails a series expansion of the end-to-end vector of the chain, Erman et al. adopted the same nonperturbation treatment and applied it to an affinely deformed network. In their model system,[12] a network was introduced as a convenience to describe and visualize the segmental orientation of the equilibrium chains in the deformed state. Erman et al. considered a deformed system and assumed that each chain extended between two active junctions that were in turn displaced affinely with the macroscopic deformation. They formulated the segmental orientation in the deformed network in terms of the second order Legendre polynomial. Of course the second-order term of the orientation distribution is the simplest possible representation and is only an approximate description.

This present work proposes an extension of the Erman et al. gaslike network theory. Starting with their model formulation, we proceed to describe the segmental orientation, not just in terms of the second-order Legendre function, but we retain the full spherical harmonic series expansion of the distribution. This is of importance in understanding the detailed deformation mechanisms of polymeric systems. For flexible polymers like polyethylene (PE) and polypropylene (PP), the gaslike theory is more suitable than the liquidlike theory. From the measured temperature dependence of the spin−lattice relaxation times (T_{1c}) by ^{13}C solid-state NMR, the value of T_{1c} for the noncrystalline component in PE becomes longer with increasing temperature.[15] This means that the amorphous state of PE exhibits char-

* To whom all correspondence should be addressed.
† Nara Women's University.
‡ Tokyo Metropolitan University.
§ Yamagata University.

10.1021/ma0007839 CCC: $22.00
Published on Web 04/27/2002

acteristics of a soft solid or a high viscosity fluid at temperatures >55 °C. For this reason, we use the Erman et al. gaslike theory to discuss the orientation function of a single element of PE corresponding to an individual crystal chain axis (the *c*-axis), and invoking kinetic nucleation theory, which considers both a surface free energy and a bulk free energy for an isolated asymmetric cluster element. The orientation of the crystal chain axes is assumed to be a kinetically determined distribution proportional to a normalized distribution of crystallite clusters present at the saddle point for the steady-state nucleation rate. In this assumption, identification of the orientations of the crystal chain axes with the orientations of the critical clusters means that the critical nuclei after formation retain their orientations in subsequent growth. By introduction of an additional approximation for the cluster critical size, the orientation of the crystal chain axes becomes proportional to the orientation distribution of single elements formed at the saddle point.

This kinetic theory is applied to analyze the orientation of crystallites within a PE film prepared by a calender process which leads to crystallization from a stressed polymer melt. For this purpose, the orientational distribution function of the crystallites is represented as a combination of the orientational distribution of the crystal chain axis (the *c*-axis) and the rotational modes of the crystallite around their *c*-axes. The calculated distribution function is then compared with the experimental one measured by X-ray diffraction. Furthermore, the light-scattering patterns under H_v polarization are calculated on the assumption that the rodlike textures in the oriented system are formed by aggregates of the clusters. The calculated and observed patterns are compared and found to be comparable.

Experimental Section

Films of low molecular weight polyethylene (LMWPE) with a viscosity average molecular weight ($\overline{M_v}$) of 5.4×10^4 were prepared by calender molding of a stressed polymer melt. The calendering method was carried out in a commercial plant. The calender film produced had a draw ratio of about 1.5, which was determined by the friction of the pair of rolls. The calender films was maintained for 15 min at 136 °C and subsequently cooled to 115 °C rapidly to facilitate its drawability. Judging from the apparent draw ratio of 1.5, the actual draw ratio of the calender film stretched up to 10 times becomes 15 times (10×1.5).

The crystallinity was calculated from the density measured by a pycnometer in chlorobenzene-toluene as a medium, by assuming the densities of the crystalline and amorphous phases to be 1.000 and 0.852 g/cm^3, respectively.[16] The melting point was estimated from the melting endotherms of the differential scanning calorimetry (DSC) curves obtained at a constant heating rate of 10 °C min^{-1}. Birefringence measurements were made using a polarizing microscope equipped with a Berek compensator to determine the retardation.

The mechanical properties were measured at room temperature with a tensile tester and a viscoelasic spectrometer (VES-F) from Iwamoto Machine Co., Ltd. The X-ray measurements were carried out using a 12 kW rotating anode X-ray generator (RDA-rA). The small-angle light-scattering (SALS) measurement with a position sensitive proportional counter (PSPC) at 200 mA and 40 kV was carried out using a point focus collimator system to determine the long period in the meridional direction. The detailed method is described elsewhere.[17,18]

The orientational distribution function of the reciprocal lattice vector of the *j*th crystal plane was estimated from the intensity distribution measured as a function of $2\theta_B$ (twice the Bragg angle) at a polar angle θ_j between the stretching direction and the reciprocal lattice vector of the *j*th crystal plane. The range of θ_j is from 0 to 90°. The intensity curve $I_{cry}(\theta_B, \theta_j)$ was decomposed into the contributions from the individual crystal planes, assuming that each peak is a symmetric Lorentzian function of $2\theta_B$ as shown in eq 1

$$I_{cry}(2\theta_B,\theta_j) = \sum_j \frac{I_j^0}{1 + (2\theta_0^{\,j} - 2\theta_B)^2/(\beta_j)^2} \tag{1}$$

where I_j^0 is the maximum intensity of the *j*th peak, β_j is the half-width of the *j*th peak, and θ_0^j is the Bragg angle at which the maximum intensity of the *j*th peak appears.

By horizontal scanning of the diffraction counter as a function of $2\theta_B$ at a given polar angle θ_j, the intensity can be determined for the *j*th crystal plane (j = (110), (200), —) and consequently the orientational distribution of the *j*th lattice vector is given by[19]

$$2\pi q_j(\cos\theta_j) = \frac{\int_{2\theta_1}^{2\theta_2} I_{cry}(\theta_B,\theta_j)\, d\theta_B}{\int_0^{\pi}\int_{2\theta_1}^{2\theta_2} I_{cry}(\theta_B,\theta_j)\, d\theta_B \sin\theta_j\, d\theta_j} \tag{2}$$

where θ_1 and θ_2 are the Bragg angles at the two feet of an isolated diffraction peak after the peak separation.[19] The orientation factor F_{l0}^j was expressed as

$$F_{l0}^{\,j} = \int_0^{\pi} 2\pi q_j(\cos\theta_j) P_l(\cos\theta_j)\, d\theta_j \tag{3}$$

The evaluation of the orientation of amorphous chain segments was obtained from the birefringence data as estimated by subtraction of crystalline contribution from the total birefringence, assuming the simple additivity proposed by Stein and Norris.[20] In doing so, the values of the intrinsic birefringence of the crystalline and amorphous phases were assumed to be 58.5×10^{-3} and 53.0×10^{-3}, respectively, which were estimated by calculation from the three principal indices of the crystal of the *n*-paraffin ($C_{36}H_{74}$) reported by Bunn and Daubeny.[21]

Light-scattering patterns were obtained with a 3 mW He—Ne gas laser as a light source. Diffuse surfaces were avoided by sandwiching the specimens between microcover glasses with silicon immersion oil having a similar index.

Theory

Following Erman et al.,[12] we consider the orientation of a reference vector **m** rigidly embedded in a chain of a deformed network. **m** makes an angle θ with respect to a laboratory-fixed axis. The mean-square cosine $\langle\cos^2\theta\rangle_{\mathbf{r}}$ of the angle θ is formulated for a chain with end-to-end vector **r** on the basis of Nagai's earlier treatment.[13] The analysis obtained by Erman et al.[12] considered only of the second moment of the orientation distribution function, and hence, the range of application was limited. To derive the orientational distribution function, we employ the geometrical arrangements and definitions proposed by Erman et al.[12] for clarity and ease of comparison with this earlier work.. For simplicity, the network chains are assumed to be monodisperse; i.e., they have the same numbers of segments. Figure 1 shows the schematic diagrams given by Erman et al.[12] Diagram a shows one configuration of a single chain, in which the vector **r** connecting two chain ends is specified with respect to the origin of the Cartesian reference frame $0{-}X_1X_2X_3$ fixed in the polymer film, the X_1 axis being perpendicular to the surface of the film, the X_3 axis being along the machine direction and X_2X_3 plane being in the plane of the film. The vector **m** makes an angle θ with respect to the X_3 axis.

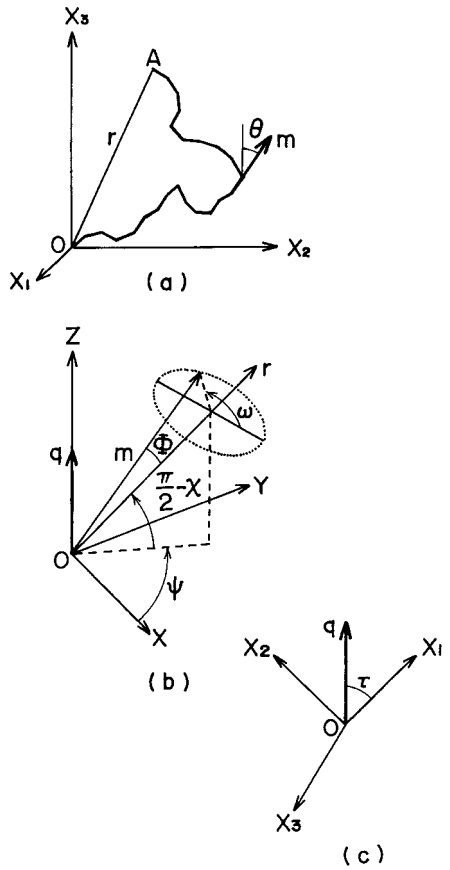

Figure 1. (a) Schematic representation of a chain OA with end-to-end vector **r**. The vector **m** is rigidly affixed to the chain and makes an angle θ with respect to Cartesian coordinate $0-X_1X_2X_3$ fixed within the film space in which the X_3 axis is the machine direction. (b) Representation of **m** and **r** in the *XYZ* coordinate system in which the *Z* axis is parallel to the transform variable **q**. Φ is the angle between **m** and **r**. φ, χ and ω are the three Euler angles. (c) Position of the transform variable q with respect to the Cartesian coordinate $0-X_1X_2X_3$ fixed within the film space. τ is the angle with respect to the X_3 axis.

Following the procedure employed by Erman et al.,[12] the nth moment $\langle\cos^n\theta\rangle_{\mathbf{r}}$ is expressed as

$$\langle\cos^n\theta\rangle_{\mathbf{r}} = Z_{\mathbf{r}}^{-1}\int\cos^n\theta\,\exp\left[\frac{-E\{\phi\}_{\mathbf{r}}}{kT}\right]\mathrm{d}\{\phi\}_{\mathbf{r}} \quad (4)$$

where $E\{\phi\}_{\mathbf{r}}$ is the energy of the configuration $\{\phi\}_{\mathbf{r}}$ defined by a set of the main chain bond rotations. The subscript **r** in $\mathrm{d}\{\phi\}_{\mathbf{r}}$ indicates that the integration is carried out with the specified end-to-end vector **r** fixed. The whole configurations space is referred to whenever the subscript **r** is omitted.[12] The symbols k and T are the Boltzmann constant and the absolute temperature, respectively. $Z_{\mathbf{r}}$ is the configurational partition function for a chain with fixed **r**, which is defined as

$$Z_{\mathbf{r}} = \int\exp\left[\frac{-E\{\phi\}_{\mathbf{r}}}{kT}\right]\mathrm{d}\{\phi\}_{\mathbf{r}} \quad (5)$$

Denoting the integral on the right-hand side of eq 4 by $f^{(n)}(\mathbf{r})$, we have

$$f^{(n)}(\mathbf{r}) \equiv \int\cos^n\theta\,\exp\left[\frac{-E\{\phi\}_{\mathbf{r}}}{kT}\right]\mathrm{d}\{\phi\}_{\mathbf{r}} = \langle\cos^n\theta\rangle_{\mathbf{r}}Z_{\mathbf{r}} \quad (6)$$

The Fourier transform $f^{(n)}(\mathbf{q})$ of $f^{(n)}(\mathbf{r})$ is

$$f^{(n)}(\mathbf{q}) = \int\mathrm{e}^{-i\mathbf{q}\cdot\mathbf{r}}\langle\cos^n\theta\rangle_{\mathbf{r}}Z_{\mathbf{r}}\,\mathrm{d}r \quad (7)$$

Here **q** is the transform variable, r is the magnitude of **r**, and χ, ψ, and ω are the three Euler angles defined in Figure 1, parts b and c.[12] In Figure 1b, *XYZ* is a new Cartesian coordinate system with the *Z* axis parallel to **q**, and the *X* axis is in the X_3Z plane. The *X* axis makes an acute angle with X_3. χ and ψ are the polar and azimuthal angles, respectively, locating **r** relative to **q** along the polar axis *Z*. The angle ω gives the rotation of the plane defined by **m** and **r** from the plane of *Y* and *Z*.

Using

$$\int_r\int_{\chi,\psi,\omega}\int_{\{\phi\}_{\mathbf{r}}}\mathrm{d}\{\phi\}_{\mathbf{r}}\sin\chi\,\mathrm{d}\chi\,\mathrm{d}\psi\,\mathrm{d}\omega\,\mathrm{d}r = 8\pi^2\int_{\mathbf{r}}\int_{\{\phi\}_{\mathbf{r}}}\mathrm{d}\{\phi\}_{\mathbf{r}}\,\mathrm{d}r = \int_{\mathbf{r}}\int_{\{\phi\}_{\mathbf{r}}}\mathrm{d}\{\phi\}_{\mathbf{r}}\,\mathrm{d}\boldsymbol{r} = \int_{\{\phi\}}\mathrm{d}\{\phi\} \quad (8)$$

Equation 7 is rewritten as

$$f^{(n)}(\mathbf{q}) = (8\pi^2)^{-1}\int_{\{\phi\}}\cos^n\theta\times\exp(-E\{\phi\}/kT)\mathrm{e}^{-i\mathbf{q}\cdot\mathbf{r}}\sin\chi\,\mathrm{d}\chi\,\mathrm{d}\psi\,\mathrm{d}\omega\,\mathrm{d}\{\phi\} \quad (9)$$

Let Φ denote the angle between **m** and **r** as shown in Figure 1b. The components of **q** along the X_1, X_2, and X_3 axes are indicated as q_1, q_2, and q_3. The angle between the X_3 axis and **q** is given by τ. From the scalar product of **m** with the X_3 axis, $\cos\theta$ can be written in terms of χ, ψ, ω, Φ, and τ as follows:

$$\cos\theta = \sin\tau[\sin\chi\cos\psi\cos\Phi + (\cos\chi\cos\psi\cos\omega - \sin\psi\sin\omega)\sin\Phi] + \cos\tau[\cos\chi\cos\Phi - \sin\chi\cos\omega\sin\Phi] \quad (10)$$

Substituting eq 10 into eq 9 and integrating over χ, ψ, and ω at fixed $\{\phi\}$, $f^n(\mathbf{q})$ (n = 2, 4, 6, and 8) can be expressed as follows:

$$f^{(2)}(\mathbf{q}) = \int\mathrm{e}^{-E/kT}\,\mathrm{d}\{\phi\}\times\left[\frac{1}{3}F_0 + F_2P_2(\Phi)P_2(\tau)\right] \quad (11)$$

$$f^{(4)}(\mathbf{q}) = \int\mathrm{e}^{-E/kT}\,\mathrm{d}\{\phi\}\times\left[\frac{1}{5}F_0 + \frac{6}{7}F_2P_2(\Phi)P_2(\tau) + F_4P_4(\Phi)P_4(\tau)\right] \quad (12)$$

$$f^{(6)}(\mathbf{q}) = \int\mathrm{e}^{-E/kT}\,\mathrm{d}\{\phi\}\times\left[\frac{1}{7}F_0 + \frac{5}{7}F_2P_2(\Phi)P_2(\tau) + \frac{15}{11}F_4P_4(\Phi)P_4(\tau) + F_6P_6(\Phi)P_6(\tau)\right] \quad (13)$$

$$f^{(8)}(\mathbf{q}) = \int e^{-E/kT}\,\mathrm{d}\{\phi\}\times\left[\frac{1}{9}F_0 + \frac{20}{33}F_2P_2(\Phi)P_2(\tau) + \frac{210}{143}F_4P_4(\Phi)P_4(\tau) + \frac{28}{15}F_6P_6(\Phi)P_6(\tau) + F_8P_8(\Phi)P_8(\tau)\right] \quad (14)$$

where F_0, F_2, F_4, F_6, and F_8 in eqs 11−14 are coefficients containing sin qr, cos qr, and qr and are given in Appendix 1. q is the magnitude of **q**. $P_n(x)$ (n = 2−8) in eqs 11−14 are Legendre polynomials. $f(\mathbf{q})$ derived by Erman et al.[12] corresponds to the second moment $f^{(2)}(\mathbf{q})$ in this paper.

Integration over configurational variables and multiplication of the denominator by $\exp(\langle r^2\rangle_0 q^2/6)$ and the numerator by the series expansion of this expression leads to

$$f^{(2)}(\mathbf{q}) = Z_0 \exp\left(\frac{-\langle r^2\rangle_0 q^2}{6}\right)\left[\frac{1}{3}K_0 + K_2L_2\right] \quad (15)$$

$$f^{(4)}(\mathbf{q}) = Z_0 \exp\left(\frac{-\langle r^2\rangle_0 q^2}{6}\right)\left[\frac{1}{5}K_0 + \frac{6}{7}K_2L_2 + K_4L_4\right] \quad (16)$$

$$f^{(6)}(\mathbf{q}) = Z_0 \exp\left(\frac{-\langle r^2\rangle_0 q^2}{6}\right)\left[\frac{1}{7}K_0 + \frac{5}{7}K_2L_2 + \frac{5}{11}K_4L_4 + K_6L_6\right] \quad (17)$$

$$f^{(8)}(\mathbf{q}) = Z_0 \exp\left(\frac{-\langle r^2\rangle_0 q^2}{6}\right)\left[\frac{1}{9}K_0 + \frac{20}{33}K_2L_2 + \frac{210}{143}K_4L_4 + \frac{28}{15}K_6L_6 + K_8L_8\right] \quad (18)$$

Here Z_0 is the configuration partition function for the free chain. The terms K_i ($i = 0-8$) and L_i ($i = 2-8$) can be expressed as power series in q, and explicit forms are given in Appendix 1. The K_i, coefficients are seen to be related to statistical averages containing $\langle r^2\rangle_0{}^m$, $\langle r^{2m}\rangle_0$, and $\langle r^{2m}P_{2n}(\cos\Phi)\rangle$ (n and m; integer), while L_i ($i = 2-8$) contain q_3 ($=q\cos\tau$) and q.

The inverse Fourier transform of eq 7 yields the required average

$$\langle\cos^n\theta\rangle_{\mathbf{r}} = (2\pi)^{-3}Z_{\mathbf{r}}{}^{-1}\int f^{(n)}(q)e^{i\mathbf{q}\cdot\mathbf{r}}\,dq \quad (19)$$

Substituting eqs 15−18 into eq 19 and performing the integration over $\mathbf{q}$ using $\mathbf{r}\cdot\mathbf{q} = xq_x + yq_y + zq_z$, gives

$$\langle\cos^n\theta\rangle_{\mathbf{r}} = C^{(n)}{}_0\left(\frac{Z_0}{Z_{\mathbf{r}}}\right)\left(\frac{3}{2\pi\langle r^2\rangle_0}\right)^{3/2} \exp\left(\frac{-3r^2}{2\langle r^2\rangle_0}\right)[1 + G + Y + Z + S + T] \quad (20)$$

where

$$G = g_4G_4 + g_6G_6 + g_8G_8 + g_{10}G_{10} + g_{12}G_{12} + g_{14}G_{14} + g_{16}G_{16} \quad (21)$$

$$Y = \eta_2Y_2 + \eta_4Y_4 + \eta_6Y_6 + \eta_8Y_8 + \eta_{10}Y_{10} + \eta_{12}Y_{12} + \eta_{14}Y_{14} + \eta_{16}Y_{16} \quad (22)$$

$$Z = z_2Z_2 + z_4Z_4 + z_6Z_6 + z_8Z_8 \quad (23)$$

$$S = s_2S_2 + s_4S_4 + s_6S_6 \quad (24)$$

$$T = t_2T_2 + t_4T_4 \quad (25)$$

The ratio $Z_{\mathbf{r}}/Z_0$ is equal to the distribution function $W(\mathbf{r})$ of the chain end-to-end vector.[13] The coefficients $C^{(n)}{}_0$ are listed in Table 1. The coefficients G_i ($i = 4-16$), Y_i ($i = 2-16$), Z_i ($i = 2-8$), S_i ($i = 2$ and 4), and T_i ($i = 2$ and 4) are found in Appendix 2 as functions of x, y, and z in addition to the statistical averages $\langle r^2\rangle_0{}^n$. The coefficients g_i ($i = 4-16$) and η_i ($i = 2-16$) are given in Appendix 2 expressed in power series of $\langle r^{2m}\rangle_0/\langle r^2\rangle_0{}^m$ ($m = 0-8$) and $\langle r^{2m}P_2(\cos\Phi)\rangle/\langle r^2\rangle_0{}^m$, respectively. z_i ($i = 2-8$), s_i ($i = 2-6$), and t_i ($i = 2-4$) are given in Appendix 1 expressed in power series in $\langle r^{2m}P_{2n}(\cos\Phi)\rangle/\langle r^2\rangle_0{}^m$. The mathematical treatment by Erman et al.[12] corresponds to $n = 2$ in eq 20, and then Z, S, and T become zero automatically. G_i are the same as β_i and Y_i is related to the α_i given by Erman et al.[12] Substituting $Z_{\mathbf{r}}/Z_0$ into eq 20, the nth moment $\langle\cos^n\theta\rangle_{\mathbf{r}}$ of the unit vector $\mathbf{m}$ can be obtained as follows:

$$\langle\cos^n\theta\rangle_{\mathbf{r}} = C^{(n)}{}_0(1 + G)^{-1}(1 + G + Y + Z + S + T) \quad (26\text{-}1)$$

$$\cong C^{(n)}{}_0(1 - G)(1 + G + Y + Z + S + T) \quad (26\text{-}2)$$

$$\cong C^{(n)}{}_0\{1 + (1 - G)Y + (1 - G)Z + (1 - G)S + (1 - G)T\} \quad (26\text{-}3)$$

It is evident that $\langle\cos^n\theta\rangle_{\mathbf{r}}$ given by eq 26 is an average for a single chain in a network with fixed end-to-end vector $\mathbf{r}$ to relate $\langle\cos^n\theta\rangle_{\mathbf{r}}$ to the observed quantities, eq 26 must be averaged over all orientations and magnitudes of the end-to-end vector. For convenience, eq 26 can be represented as a function of three components, x, y, and z of the end-to-end vector $\mathbf{r}$ in the deformed state, since all the coefficients in eq 26 are composed of the term r^{2m}. Hence, the mathematical treatment of the nth moment can be carried out using the same method as proposed by Erman et al. for the second moment.[12] Assuming an affine deformation, the quantity $x^py^qz^r$ can be related to the quantity in the undeformed state by

$$x^py^qz^r = \lambda_x{}^p\,\lambda_y{}^q\,\lambda_z{}^r\,x_0{}^p\,y_0{}^q\,z_0{}^r \quad (27)$$

where λ_x, λ_y, and λ_z are the X_3, X_2, and X_1 components of λ. For uniaxial stretching, we have

$$\lambda_x = \lambda, \quad \lambda_y = \frac{1}{\lambda}, \quad \lambda_z = \frac{1}{\lambda}(\lambda\text{: draw ratio}) \quad (28)$$

When the chain end-to-end vector is specified in terms of a polar angle θ and an azimuthal angle φ, the undeformed components may in turn be expressed as

$$\begin{aligned} x_0 &= r_0\cos\theta \\ y_0 &= r_0\sin\theta\cos\varphi \\ z_0 &= r_0\sin\theta\sin\varphi \end{aligned} \quad (29)$$

By following the treatment by Erman et al.,[12] we find

Table 1. Values of $C_i^{(n)}$

	$C_i^{(n)}$				
n	$i = 0$	$i = 2$	$i = 4$	$i = 6$	$i = 8$
2	1/3	1	0	0	0
4	1/5	6/7	1	0	0
6	1/7	5/7	15/11	1	0
8	1/9	20/33	210/143	28/15	1

$$\langle \cos^n \theta \rangle = C^{(n)}{}_0[1 + D_1(\lambda^2 - 1/\lambda^{-1}) + D_2(\lambda^4 + {}^1/_3\lambda - {}^4/_3\lambda^{-2}) + D_3(\lambda^6 + {}^3/_5\lambda^3 - {}^8/_5\lambda^{-3}) + D_4(\lambda^8 + {}^5/_7\lambda^5 + 12/35\,\lambda^2 - 8/35\,\lambda^{-1} - 64/35\,\lambda^{-4}) + E_2(\lambda^4 - 2\lambda + \lambda^{-2}) + E_3(\lambda^6 - {}^4/_5\lambda^3 + {}^6/_5\lambda^{-3} - 7) + E_4(\lambda^8 - {}^2/_7\lambda^5 - 37/35\,\lambda^2 - 36/35\,\lambda^{-1} + 48/35\,\lambda^{-4}) + F_3(\lambda^6 - 3\lambda^3 - \lambda^{-3} + 3) + F_4(\lambda^8 - 13/7\,\lambda^5 - {}^3/_7\lambda^2 + 17/7\,\lambda^{-1} - {}^8/_7\lambda^{-4}) + H_4(\lambda^8 - 4\lambda^5 + 6\lambda^2 - 4\lambda^{-1} + \lambda^{-4})] \quad (30)$$

where D_j ($j = 1-4$) and E_j ($j = 2-3$) are expressed as a function of the product of g_i ($i = 4-16$) and η_i ($i = 2-16$) and the product of g_i ($i = 4-10$) and z_i ($i = 2-8$), respectively. F_j ($j = 3-4$) and H_4 are also expressed as a function of the product of g_i ($i = 4-10$) and s_i ($i = 2-6$) and the product of g_i ($i = 4-10$) and t_i ($i = 2-4$), respectively. All of these coefficients are found in Appendix 3. When all the coefficients except g_i ($i = 4$, 6, and 8) and η_i ($i = 2$, 4, 6, and 8) are put equal to zero, then E_2, E_3, E_4, F_3, F_4, and H_4 also reduce to zero. In this case, eq 30 reduces to the second-order moment $\langle \cos^2\theta \rangle$ derived by Erman et al. (see eq 28 in ref 12).

Using $\langle \cos^n \theta \rangle$ in eq 30, the orientational distribution function $w_{am}(\cos\theta)$ of the segments with respect to the Cartesian reference frame $0-X_1X_2X_3$ can be represented as a series of Legendre polynomials, i.e.,

$$2\pi\omega_{am}(\cos\theta) = \frac{1}{2} + 2\sum_{l=2}^{8}\frac{2l+1}{2}F_{l00}P_l(\cos\theta) \quad (31)$$

where $P_l(\cos\theta)$ is the Legendre polynomials and F_{l00} is the lth order orientation factor given by

$$F_{200} = \frac{1}{2}(3\langle\cos^2\theta\rangle - 1) \quad (32\text{-}1)$$

$$F_{400} = \frac{1}{8}(35\langle\cos^4\theta\rangle - 30\langle\cos^2\theta\rangle + 3) \quad (32\text{-}2)$$

$$F_{600} = \frac{1}{16}(231\langle\cos^6\theta\rangle - 315\langle\cos^4\theta\rangle + 105\langle\cos^2\theta\rangle - 5) \quad (32\text{-}3)$$

$$F_{800} = \frac{1}{128}(6435\langle\cos^8\theta\rangle - 12012\langle\cos^6\theta\rangle + 6930\langle\cos^4\theta\rangle - 1260\langle\cos^2\theta\rangle + 35) \quad (32\text{-}4)$$

The statistical averages $\langle r^n \cos^n \Phi\rangle_o$ (represented as $\langle r^n P_n(\cos\Phi)\rangle$) and $\langle r^2\rangle_o{}^n$ must be evaluated to carry out numerical calculations. This can be accomplished by assuming independent rotations of each chain. In one approach, Erman et al. adopted Monte Carlo averaging. To pursue an analytical treatment, we will assume $\langle r^n \cos^n \Phi\rangle_o$ may be factored $\langle r^n\rangle_o\langle\cos^n\Phi\rangle_o$ and also we will adopt the freely jointed chain model to evaluate $\langle r^n\rangle_o/\langle r^2\rangle_o{}^n$ ($\langle r^2\rangle_o = mb^2$, where m is the number of freely jointed statistical segments and b is the bond length). As pointed out by Flory,[14] the Fourier transform $G(\mathbf{q})$ of $W(\mathbf{r})$ ($=Z_{\mathbf{r}}/Z_0$) is given by

$$G(q) = \left[\frac{\sin(qb)}{qb}\right]^m = 1 - \left[\frac{m}{3!}\right]b^2q^2 + \left[\frac{m(m-1)}{2(3!)^2} + \frac{m}{5!}\right]b^4q^4 - \left[\frac{m(m-1)(m-2)}{3!(3!)^3} + \frac{m(m-1)}{3!5!} + \frac{m}{7!}\right]b^6q^6 + \ldots \quad (33)$$

On the other hand, $G(\mathbf{q})$ is given by the power series

$$G(q) = \int_0^\infty \frac{4\pi r^2 W(r)}{qr}\sin(qr)\,dr = \int_0^\infty \left(1 - \frac{q^2r^2}{3!} + \frac{q^4r^4}{5!} - \ldots\right)4\pi r^2 W(r)\,dr = 1 - \frac{\langle r^2\rangle_0}{3!}q^2 + \frac{\langle r^4\rangle_0}{5!}q^4 - \frac{\langle r^6\rangle_0}{7!}q^6 + \ldots \quad (34)$$

The quantity $\langle r^n\rangle_o/\langle r^2\rangle_o{}^n$ was obtained up to the 16th order by comparing the coefficients of q^n in eqs 33 and 34.

The value of $\langle \cos^n \Phi\rangle_o$ was estimated as the nth moment of the Langevin function as follows:

$$\langle \cos^n\Phi\rangle_0 = \frac{\int_0^\infty\int_0^\pi W(r)f(\Phi,r)\cos^n\Phi\sin\Phi\,d\Phi\,dr}{\int_0^\infty\int_0^\pi W(r)f(\Phi,r)\sin\Phi\,d\Phi\,dr} \quad (35)$$

where

$$f(\Phi,r) = \frac{1}{2}\left\{\frac{\beta}{\sinh\beta}\right\}\exp\{\beta\cos\Phi\} \quad (36)$$

and β becomes

$$\beta = 3\left(\frac{r}{mb}\right) + \frac{9}{5}\left(\frac{r}{mb}\right)^3 + \frac{297}{175}\left(\frac{r}{mb}\right)^5 + \ldots \quad (37)$$

where m is the number of freely jointed statistical segments and b is the bond length.

Figure 2 shows the second-order orientation factor, F_{200}, as a function of draw ratio (λ). In actual calculations, the number of chain segments was fixed to be $m = 20$ and 100. Three graphs, a–c, represent the termination effect of the coefficients, g_i and η_i with $D_4 = 0$, while graph d shows the orientation factor calculated up to the 12th order of g_i and η_i for finite $D_4 \neq 0$. Graph a shows the same profile as obtained by Erman et al. with the same terms g_i and η_i (see Figures 6 and 7 in ref 12). This indicates that simple factorization of $\langle r^n\rangle_o/\langle r^2\rangle_o{}^n$ using a freely jointed chain model and $\langle \cos^n\Phi\rangle_o$ obtained as the nth moment of the Langevin function is almost equal to $\langle r^n \cos^n\Phi\rangle_o/\langle r^2\rangle_o{}^n$ as calculated by a Monte Carlo method. Furthermore, as shown in graphs b and c, the curves become sharper with an increase in the number of terms. The orientation factor exceeds unity with increasing draw ratio and this tendency becomes considerable with decreasing m. The term D_4 is very sensitive to the curve profile. D_1 is on the order of m^{-1}, D_2 and D_3 are on the order of m^{-2}, while D_4 is on the order of m^{-3}. The coefficient D_4 introduces the effect of λ^8 which favors negative values of the orientation factor. Actually this tendency becomes more pronounced with increasing draw ratio, indicating the considerable preferential orientation of chain segments perpendicular to the machine direction. Such behavior is in contradiction to the model in Figure 1 and also

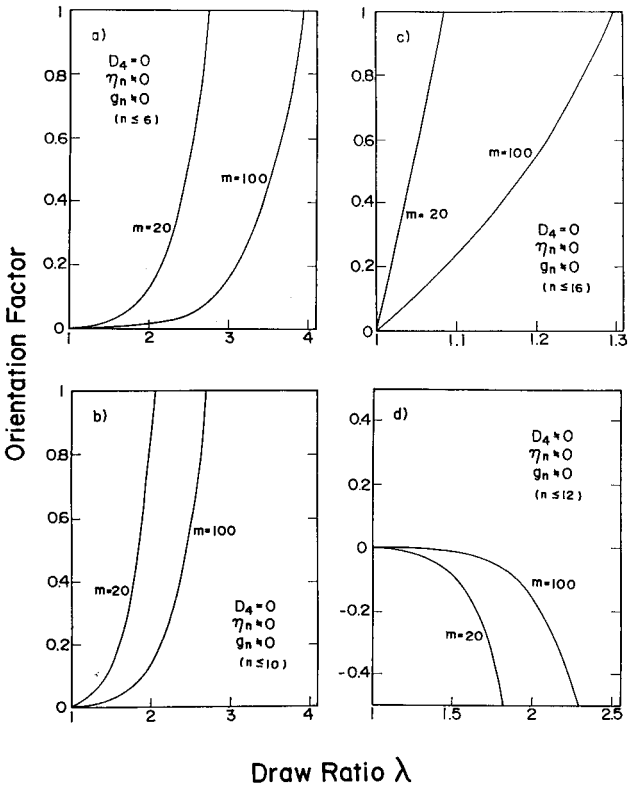

Figure 2. Second-order orientation factor vs draw ratio (λ) calculated for the number of chain segments of $m = 20$ and 100: (a) $\eta_i \neq 0$ and $g_i \neq 0$ at $i \leq 6$ and $D_4 = 0$, (b) $\eta_i \neq 0$ and $g_i \neq 0$ at $i \leq 10$ and $D_4 = 0$, (c) $\eta_i \neq 0$ and $g_i \neq 0$ at $i \leq 16$ and $D_4 = 0$, and (d) $\eta_i \neq 0$ and $g_i \neq 0$ at $i \leq 12$ and $D_4 \neq 0$.

deviates from experimental results which have been observed for most drawn polymer films and fibers. Accordingly, the contribution of the D_4 term, as described by Erman et al., [12] remains close to zero for smaller deformations. The position of the curves that deviate from zero appears at higher extension ratios with increasing value of m. For example, the contribution of the D_4 term at $m = 100$ will be negligible up to fairly large extension ratios. Therefore, one can establish the limits of validity of the extension ratio for a given m value, by looking at where the contribution of the D_4 term starts to deviate from zero in the negative direction.

Figure 3 shows the orientation distribution functions calculated using eq 31 at the indicated draw ratio. The parameters needed to calculate the curves in the four graphs, a−d, were the same as those used in the corresponding graphs in Figure 1. The orientation functions have a maximum at $\theta = 0°$ and the profiles become sharper with increasing terms of g_i and η_i. In contrast, the curves at $D_4 \neq 0$ show a maximum value at $\theta = 90°$ denoting the inverse orientation behavior. As shown in Figure 3, the orientational distribution functions calculated at $m = 20$ up to the 16th order of g_i and η_i exhibits a very sharp profile at $\lambda = 1.02$. Such a sharp profile, however, has never been observed for drawn polymer films. Experimental orientation functions at low draw ratios such as $\lambda = 1.02$ are almost independent of the polar angle θ, indicating a very small orientation of the chain segments.

We emphasize that this unphysical behavior for $D_4 = 0$ is due to the use of eq 26−3 as an approximation to eq 26−1 for $\langle \cos^n \theta \rangle$. If eq 26−1 was adopted instead of eq 26−3, appropriate numerical results will result. New

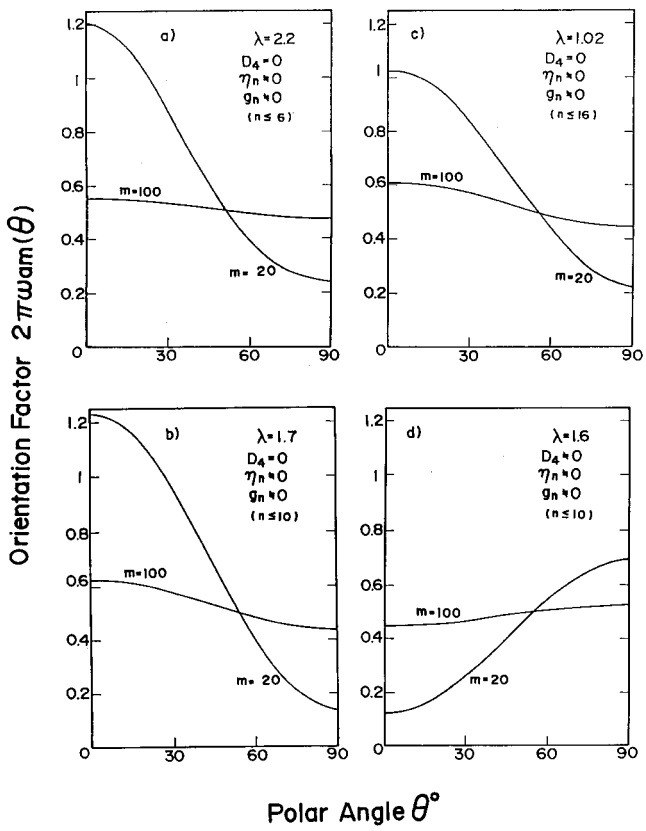

Figure 3. Orientation distribution functions calculated for the number of chain segments of $m = 20$ and 100: (a) $\eta_i \neq 0$ and $g_i \neq 0$ at $i \leq 6$ and $D_4 = 0$ at $\lambda = 2.2$, (b) $\eta_i \neq 0$ and $g_i \neq 0$ at $i \leq 10$ and $D_4 = 0$ at $\lambda = 1.7$, (c) $\eta_i \neq 0$ and $g_i \neq 0$ at $i \leq 16$ and $D_4 = 0$ at $\lambda = 1.02$, and (d) $\eta_i \neq 0$ and $g_i \neq 0$ at $i \leq 12$ and $D_4 \neq 0$ at $\lambda = 1.6$.

Table 2. Characteristics of the Original Calender Film and the Drawn Film

		calender film	drawn film
melting point (°C)		134	137
crystallinity (%)		70.2	79.1
identity period (Å)		220	350
Young's modulus (GPa)		1.6	28.0
orientation factor (F_{200})	*a*-axis	0.251	−0.401
	b-axis	−0.357	−0.430
	c-axis	0.113	0.831
	amorphous segments	−0.045	0.815

approaches to computing $\langle \cos^n \theta \rangle$ directly from eq 26−1 are clearly needed..

Application to Polyethylene

We consider the effect of amorphous chain segments on induced crystallization[22,23] as an application of the theory and to assess its utility. We begin with the theory of crystal nucleation from oriented cylindrical elements, which stipulates that it is necessary to have a common orientation of a growing cluster and colliding single element as the condition for cluster growth. Before discussing the analysis, we mention briefly the properties of the two kinds of test specimens employed experimentally.[11] The original calender films and drawn films were both used as test specimens and their characteristics are listed in Table 2. The melting points, the volume crystallinities, and the Young's moduli of the drawn films at 20 °C are all higher than the corresponding properties of the original (undrawn)

calender films. The Young's modulus of a drawn film was 28 GPa. As described in our previous paper,[11] the Young's moduli of calender films with viscosity average molecular weights of $\overline{M_v} = 70\,000$ were less than 16 GPa even after drawing up to 21 times. This implies the importance of rapidly cooling from 136 to 115 °C before drawing (see Experimental Section). Incidentally, the Young's modulus of the present calender film is almost equal to that (30GPa) of ultrahigh molecular weight polyethylene films ($\overline{M_v} = 6 \times 10^6$) which were prepared by gelation/crystallization from solution and stretched up to 50 times.[19]

Now, we consider the orientation-induced crystallization of the original calender film. For this purpose, we define a kinetically determined distribution $W_c(\theta)$ of crystal chain axes as the normalized distribution of clusters found at the saddle point corresponding to a nonuniform orientation distribution under conditions of a steady-state nucleation rate.[24] In this viewpoint, the identification of the orientation of the *c*-axis with that of the critical cluster means that the critical nuclei after formation retain their original orientation in the subsequent growth. Thus,

$$W_c(\theta) = \text{const}\ \omega_{am}(\cos\theta)\exp\left[-\frac{\Delta F(r^*,l^*,\theta)}{kT}\right] \qquad (38)$$

where r^* and l^* are the critical cylinder radius and length and $\Delta F(r^*, l^*, \theta)$ is the free energy at the saddle point, associated with the effective driving force of the cluster growth. In eq 38, the free energy needed to form a cylindrical cluster is given by

$$\Delta F(r,l,\theta) = 2\pi r^2\sigma_e + 2\pi rl\sigma_s + \pi r^2 l\left[\Delta f - \left(\frac{kT}{v_0}\right)\ln\chi(\theta)\right] \qquad (39)$$

where σ_e and σ_s are the end and the side surface free energies of polyethylene having values of 6.75×10^{-6} and 1.3×10^{-6} J/cm^2, respectively[25], Δf is the bulk free energy of cluster formation, and v_0 is the volume of a single element. $\chi(\theta)$ is proportional to the probability of finding a single element oriented at an angle θ within some finite tolerance range and is nearly equal to $w_{am}(\theta)$ denoting the orientation function of single chain elements. Substituting $\Delta F(r^*,l^*,\theta^*)$ into eq 38, we have

$$W_c(\theta) = C\omega_{am}(\cos\theta)\exp\left[\frac{-8\pi\sigma_e{\sigma_s}^2}{D(\theta)^2 kT}\right] \qquad (40)$$

where C is the normalization constant. The orientation-dependent function $D(\theta)$ can be obtained by using $w_{am}(\cos\theta)$ in eq 31 as follows:

$$D(\theta) = \Delta f - \left(\frac{kT}{v_0}\right)\ln\chi(\theta)\ \Delta f - \left(\frac{kT}{v_0}\right)\ln[4\pi\omega_{am}(\cos\theta)] \qquad (41)$$

Assuming Kuhn−Grün statistics for the segmental orientation,[4] we have

$$\Delta f = \Delta f|_{\lambda=1} - \left(\frac{kT}{2N_s v_0}\right)\left(\lambda^2 + \frac{2}{\lambda} - 3\right) \qquad (42)$$

where $\Delta f|_{\lambda=1}$ is given by $\Delta h\ (T - T_m^o)/T_m^o$, where Δh is the density of the heat of fusion and T_m^o is the equilibrium melting point.

In numerical calculations, the following values of the parameters were used: the enthalpy of melting per mole of statistical segments, 4.03 kJ/mol;[26] the equilibrium melting point, 137.5 °C; [26] and the number of statistical segments, $m = 100$. The volume v_0 ($=\pi r^2 l$) of a single kinetic element is an unknown parameter, but the calculated results in the range $(2-4) \times 10^{-22}$ cm^3 were insensitive to the value used. Accordingly, we adopted the value 3×10^{-22} cm^3, which is similar to the value for rubber,[27] as discussed in our previous work.[11]

Crystalline polymers are generally heterogeneous and are composed of polymer chains aggregated randomly to form amorphous regions along with more or less regular regions comprising several different orders of crystalline structural units. Therefore, deformations such as rotation of a crystal unit due to straining of tie-chains must be taken into consideration in addition to the simple orientation of the *c*-axis given in eq 40. If the orientation of the crystallites actually followed a random orientation around the *c*-axis as given by eq 40, then all of the orientational distribution functions for the (h k 0) planes would show the same profile. However, the observed X-ray patterns for the (h k 0) planes have unique characteristics for drawn polyethylene films and the present specimens also exhibit this characteristic behavior as is discussed below. A possible source of the rotational distortion is provided by the strain energy of anisotropic crystallites in a stress field in a deformed network. Considering this mechanism, a complete description of the orientation of the crystallites may be specified by using three Eulerian angles, ϕ, θ, and η as shown in diagram a in Figure 4. The angles θ and ϕ, which define the orientation of the *c*-axis relative to the laboratory frame, are the polar and azimuthal angles, respectively, and η specifies the rotation of the crystal unit around the *c*-axis. Under uniaxial orientation, the orientation function is independent of ϕ. Thus, the orientation distribution function of the crystallites in the deformed sample may be formulated empirically by allowing rotation of the crystallites around the *c*-axis as follow leading to the distribution:

$$\omega(\theta,\eta) = C_0 W_c(\theta)\{1 + \sigma_1(\lambda - 1)\sin^{2J_A}\theta\cos^{2J_C}\eta + \sigma_2(\lambda - 1)(\sin\theta\cos\theta)^{2J_B}\cos^{2J_D}\eta + \sigma_3(\lambda - 1)\cos^{2J_E}\eta + \sigma_4(\lambda - 1)\cos^{2J_F}\eta\} \qquad (43)$$

where C_0 is the normalization constant. Equation 43 is based on our prior works.[11] This expression contains 10 fitting parameters which are determined from the numerical fits to the scattering data (see below). The second and third terms on the right-hand side of eq 43 represent the rotation of the crystallites around the *c*-axis, and they have significant contributions at $\theta =$ 90 and 45°. Of course, through such rotations, the crystalline *a*-axes acquire the greatest opportunity to be in the plane formed by the *c*-axis and the machine direction. With increasing values of the parameters J_A and J_B, the possibility of finding crystallites becomes higher at $\theta = 0°$ and 90°, respectively. The fourth and the fifth terms denote the rotations independent of the polar angle θ. The parameters σ_1, σ_2, σ_3, and σ_4 express the ease of the rotation, and J_C, J_D, J_E, and J_F represent the sharpness of the distribution. The expression for eq 43 was limited to a maximum of five terms in the present instance for simplicity.

As discussed in a previous paper,[11] the orientation factors F_{l0n} of the crystallites may be obtained as follows:

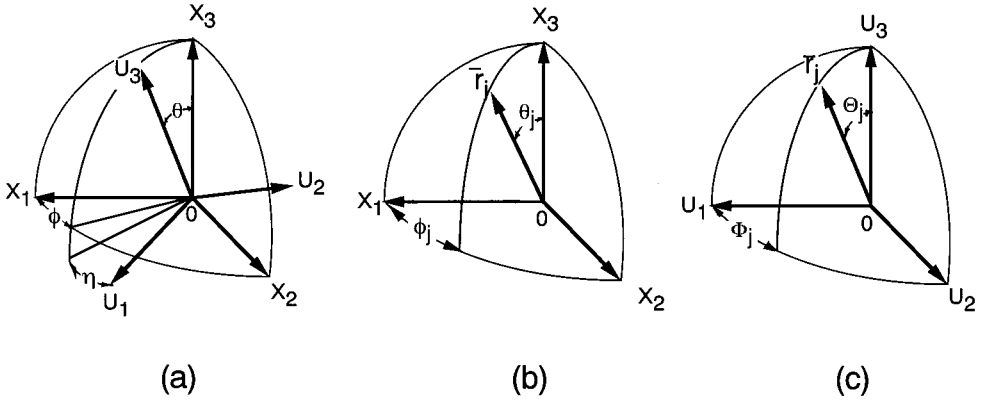

Figure 4. Cartesian coordinate illustrating the geometrical relation: (a) Euler angles θ and η which specify the orientation of coordinate $0-U_1U_2U_3$ of structural unit with respect to coordinate $0-X_1X_2X_3$ of specimen; (b) angles θ_j and ϕ_j which specify the orientation of the given jth axis of the structural unit with respect to the coordinate $0-X_1X_2X_3$, (c) angles Θ_j and Φ_j which specify the orientation of the jth axis of the structural unit with respect to the coordinate $0-U_1U_2U_3$.

$$F_{l0n} = \int_0^{2\pi}\int_0^{\pi} \omega(\theta,\eta)P_l^{\,n}(\cos\theta)\cos n\eta \sin\theta \mathrm{d}\theta d\eta \quad (44)$$

The orientation factor $F_{l0}^{\,j}$ of the jth crystal plane can be obtained by using F_{l0n},

$$F_{l0}^{\,j} = F_{l00}P_l^{\,n}(\cos\Theta_j) + 2\sum_{n=2}^{l}\frac{(l-n)!}{(l+n)!}F_{l0n}P_l^{\,n}(\cos\Theta_j)\cos n\Phi_j \quad (45)$$

where Θ_j and Φ_j are the polar and azimuthal angles specifying the orientation of the reciprocal lattice vector with respect to the Cartesian coordinate of a crystal unit.[2] Thus, the orientation distribution function $2\pi q_j(\cos\theta_j)$ of the reciprocal lattice vector of the jth crystal plane is obtained by substituting eq 45 into the following equation:

$$2\pi q_j(\cos\theta_j) = \frac{1}{2} + 2\sum_{l=2}^{\infty}\frac{2l+1}{2}F_{l0}^{\,j}P_l(\cos\theta_j) \quad (46)$$

Incidentally, the detailed geometrical arrangements for θ_j in eq 46 and Θ_j and Φ_j in eq 45 are shown in Figure 4, parts b and c, respectively.

The functions $2\pi q_j(\cos\theta_j)$ are available directly using X-ray diffraction techniques as described in the Experimental Section, and the adequacy of the present model can be judged by comparing the theoretical and experimental results for $2\pi q_j(\cos\theta_j)$. In doing so, the experimental accuracy of the measured values of $2\pi q_j(\cos\theta_j)$ must be estimated. The estimation method which we use was proposed by Roe and Krigbaum.[1,2] As a first step, the generalized orientation factors F_{l0n} are determined by solving the linear system of eq 45 containing $F_{l0}^{\,j}$ using a least-squares method, in which $F_{l0}^{\,j}$ corresponds to the lth order orientation factor of the jth crystal plane obtained by eq 3 experimentally. Thus, $F_{l0}^{\,j}$ calculated using F_{l0n} leads to $2\pi q_j(\cos\theta_j)$ from eq 46. The resulting calculated curves must be in good agreement with those from eq 3 obtained experimentally by X-ray diffraction measurements. Unless one confirms the accuracy of the experimental data, of course, subsequent comparisons between the experimental and the theoretical results from will be meaningless.

For this purpose, weighting factors ρ_j were introduced to determine F_{l0n} from eq 45 by a least-squares method. The values of ρ_j were assumed initially to be nearly proportional to square of the structure factor and were subsequently varied to obtain the best fit between experimental and calculated results by the simplex method. A mean-square error between the calculated $F_{l0}^{\,j}$ and recalculated $F_{l0}^{\,j}$ was obtained using:

$$R = \frac{\sum_j\sum_l \rho_j[(F_{l0}^{\,j})_{\mathrm{cal}} - (F_{l0}^{\,j})_{\mathrm{recal}}]^2}{\sum_j\sum_l \rho_j[(F_{l0}^{\,j})_{\mathrm{cal}}]^2} \quad (47)$$

As described above, we recalculated $F_{l0}^{\,j}$, in turn, from the values of F_{l0n}, and further calculated $2\pi q_j(\cos\theta_j)$ using eq 46 to minimize the value of R in eq 47. The value of R in eq 47 was 9.2%.

Figure 5 shows the observed orientation functions $2\pi q_j(\cos\theta_j)$ (open circles) with the calculated functions (dotted curves). The recalculated functions are in very good agreement with the observed functions. This indicates that the experimental functions have high accuracy and consequently the comparison between the experimental result and the theoretical result calculated by eq 43 associated with the model system shown in Figure 1 can be justified. The theoretical $2\pi q_j(\cos\theta_j)$ are shown as solid curves in Figure 5. The numerical calculation was continued until a best fit was achieved within the capacity of the simplex method.[28] As a result, the following parameters yielded the best fit: $\sigma_1 =$ 28 662, $\sigma_2 = 24$, $\sigma_3 = 20$, $\sigma_4 = 7854$, $J_A = 1$, $J_B = 36$, $J_C = 11$, $J_D = 2$, $J_E = 12$, and $J_F = 12$. These parameters indicate that several kinds of rotational motions of the crystallites arise due to the preferential orientation of the c-axes with respect to the stretching direction. For example, the large values of σ_1 and σ_4 with $J_A = 1$ and $J_F = 12$ suggest that the predominant orientational disposition of the crystallites involves a dull or indistinct rotational preference around the c-axis in the transverse direction plus a sharp rotation independent of the polar angle θ. Equation 46 truncated at $l = 8$ gives good agreement with the observed distribution functions, even for the less accurately superimposed crystal planes with lower X-ray diffraction intensity. This agreement helps to justify the network model in Figure 1 as well as the kinetic theory for the orientation of the crystal chain axis discussed above.

In a previous paper,[11] similar orientation distributions of reciprocal lattice vectors were observed for calender

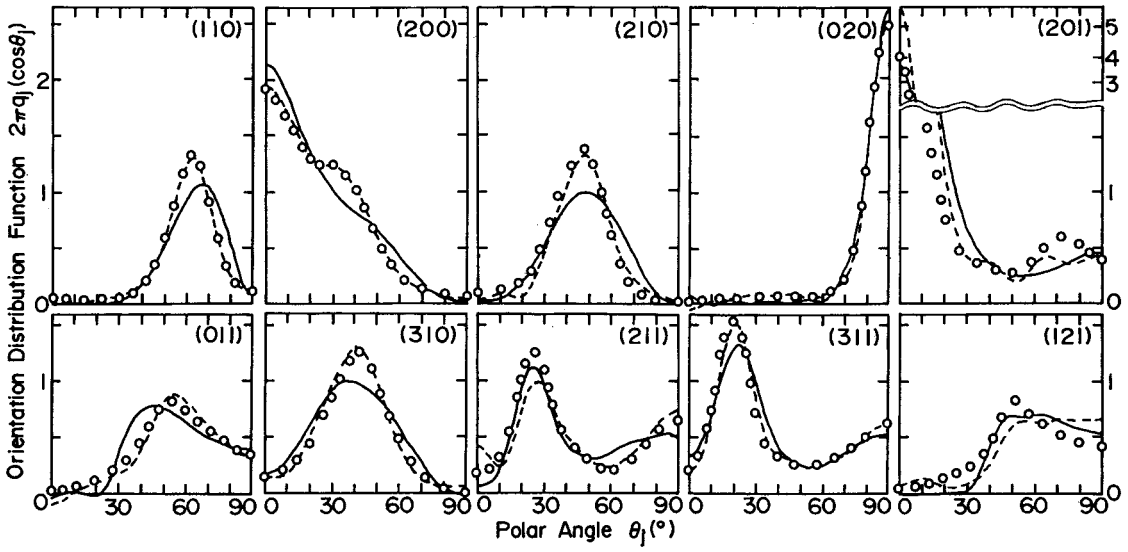

Figure 5. Orientation distribution functions $2\pi q_j(\cos\theta_j)$ of the reciprocal lattice vectors of the indicated crystal planes of the PE calender film. Circles: values of $2\pi q_j(\cos\theta_j)$ obtained from experimental measurements. Dashed curves: values of $2\pi q_j(\cos\theta_j)$ calculated with the 19-term series (l up to 18) with the use of reconstructed $F_{l0}{}^j$. Solid curves: $2\pi q_j(\cos\theta_j)$ calculated from eq 43 (l up to 8).

films ($\lambda = 1.5$), with viscosity-average molecular weights of PE equal to 7×10^4, prepared by calendaring two rolls at 65 and 125 °C, respectively. The theoretical curves calculated using a liquidlike theory were in good agreement with the observed results. Despite this previous good agreement, the liquidlike theory used formerly assumes a liquid crystalline ordering caused by chain stiffness. The good agreement in the present paper is more rigorous in comparison with the previous treatment,[11] since the present gaslike theory is the most appropriate way to estimate the orientational behavior polyethylene having flexible amorphous chain mobility.

To facilitate an understanding of the mechanism of orientation-induced crystallization in the calender films, further discussion is now presented in terms of the orientation distribution function $\omega(\cos\theta, \eta)$ of crystallites. The orientation distribution function $\omega(\cos\theta, \eta)$ of the crystallites can be calculated from the recalculated $2\pi q_j(\cos\theta_j)$ as follows;

$$\omega(\cos\theta,\eta) = \frac{1}{2} + 2\sum_{l=2}\frac{2l+1}{2}\left[F_{l00}P_l(\cos\theta) + 2\sum_{n=2}\frac{(l-n)!}{(l+n)!}F_{l0n}P_l^m(\cos\theta)\cos n\eta\right] \quad (48)$$

where l is limited to 18.

This function can be calculated from eq 43 by using parameters determined by the best fitting between experimental and theoretical curves of $2\pi q_j(\cos\theta_j)$.

Parts a and b of Figure 6 show theoretical and experimental maps of the orientational distribution function $\omega(\theta,\eta)$, respectively. Map a is obtained from eqs 43, 44, 45, and 48 and is shown to check the termination error due to truncation of the spherical harmonics at the eighth order. Map b is obtained by substituting F_{l0n} into eq 48. On the basis of the recalculated $F_{l0}{}^j$, F_{l0n} are determined by solving the linear equation of eq 45. In map a, there exist several negative regions (black zones) due to series termination error. On the other hand, the negative regions in map b are due to artifacts associated with termination errors of the spherical harmonics up to $l = 18$. From the appearance of the negative regions,

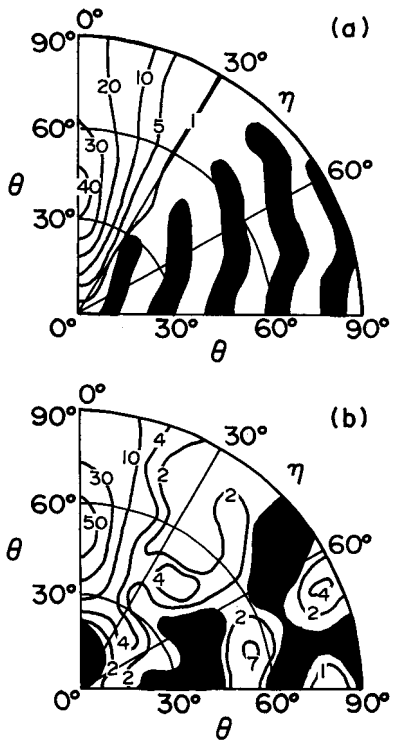

Figure 6. Orientation distribution functions of PE crystallites within the calender film: (a) contour map calculated from eq 65 (l up to 8) through eqs 43−45; (b) contour map calculated with the 19-term series (l up to 18) with the use of reconstructed $F_{l0}{}^j$.

one sees that the sharper the orientation distribution of $2\pi q_j(\cos\theta_j)$ is, the more negative regions result. It is seen that map a has a populated region at $\theta = 40°$ and $\eta = 0°$, while map b has a populated region at $\theta = 50°$ and $\eta = 0°$. This means that the orientation distribution function of the crystallites in the original calender film ($\lambda = 1.5$) may be approximately expressed using eq 43. This supports the representation of the orientation of the crystallites as a combination of a kinetically determined orientation around the c-axis plus a rotational redistribution of the crystallites around their c-axes. In

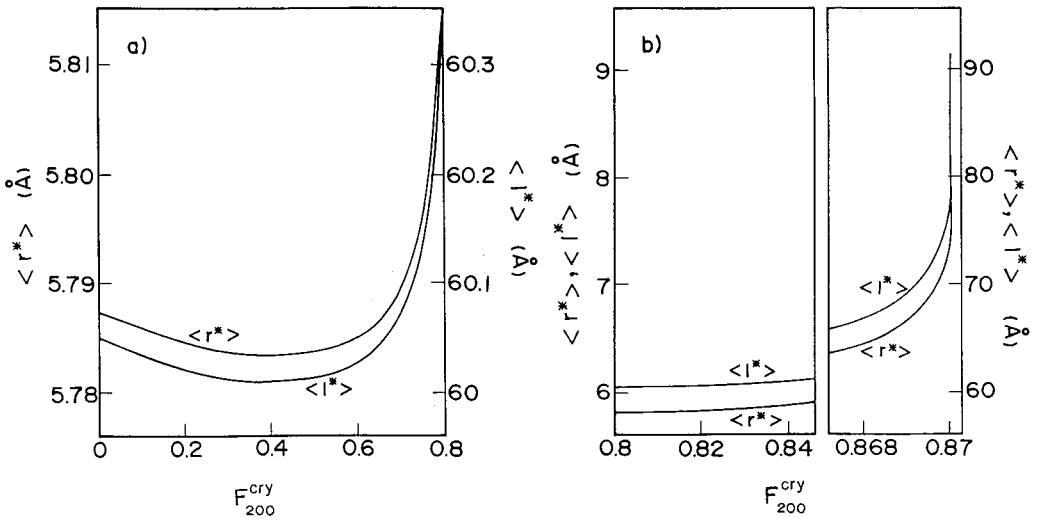

Figure 7. Average critical values of r^* and l^* averaged by polar angle against the second-order orientation factor F_{200}^{cry} of the c-axis obtained from eq 40.

map a, a highly populated area at $\eta = 0°$ indicates rotation of the crystallites around their own c-axes arising from the $\cos^{2p}\eta$ terms in eq 43. Another populated area at $\theta = 40°$ reflects the orientation of the c-axes arising chiefly from the front factor $W(\theta)$, but including influences of the other terms as well..

Application to the Analysis of Light-Scattering Patterns

As discussed before, the free energy of the formation of a crystalline cluster in a liquid or amorphous phase, ΔF, is given by eq 39 according to crystallization theory by Ziabicki.[22,23] In this case, the critical radius r^* and the critical length l^* of a cylindrical crystal element can be determined from the condition that the first-order derivative of ΔF is zero at the saddle point and they are given as a function of the polar angle θ in Figure 1a (or Figure 4a). Namely, their sizes $r^*(\theta)$ and $l^*(\theta)$ are related to the orientation distribution function $W_c(\theta)$ of the elements. Hence the average critical values, $\langle r^* \rangle$ and $\langle l^* \rangle$ are given as follows:

$$\langle r^* \rangle = \frac{1}{2}\int_0^\pi W_c(\theta) r^*(\theta) \sin\theta \, d\theta \tag{49}$$

$$\langle l^* \rangle = \frac{1}{2}\int_0^\pi W_c(\theta) l^*(\theta) \sin\theta \, d\theta \tag{50}$$

Of course, $r^*(\theta)$ and $l^*(\theta)$ are given as a function of λ. For simplification, we estimate $\langle r^* \rangle$ and $\langle l^* \rangle$ against the second-order orientation factor F_{200}^{cry} of the elements given by

$$F_{200}^{cry} = \frac{1}{2}\int_0^\pi W_C(\theta) P_2(\cos\theta) \sin\theta \, d\theta \tag{51}$$

where $W_c(\theta)$ was given in eq 38, in which $w_{am}(\theta)$ given as eq 31 is represented up to the 10th order of g_i and η_i at $D_4 = 0$ and the values of F_{200}^{cry} in eq 51 were calculated by adopting λ used on calculating $\langle r^* \rangle$ and $\langle l^* \rangle$.

Figure 7 shows results. It is seen that $\langle r^* \rangle$ and $\langle l^* \rangle$ are very sensitive to F_{200}^{cry}. Both $\langle r^* \rangle$ and $\langle l^* \rangle$ decrease slightly with increasing F_{200}^{cry} and take their minimum at around 0.4. $F_{200}^{cry} > 0.6$, however, the values increase drastically, indicating that the crystallite size becomes extremely larger with increasing the orientational degree of crystallite. On the basis of the above information, small-angle light scattering under H_v polarization condition is calculated using the present kinetic theory in order to compare with the observed pattern from the polyethylene film which was prepared by calendering from the shear-stressed polymer melt.

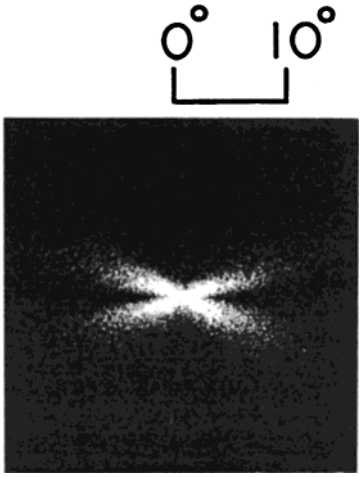

Figure 8. H_v light-scattering patterns from the calender film.

Figure 8 shows a small-angle light-scattering pattern from the original calender film ($\lambda = 1.5$) under H_v polarization condition. The pattern shows X-type lobes whose intensity has a maximum in the scattering center and decrease monotonically with increasing scattering angle. This indicates the existence of rods oriented in the machine direction.[29] To analyze the formation of rodlike textures in an oriented-induced crystallization system, we shall propose a model shown in Figure 9. In this model system, a rod represents an aggregate of a number of clusters (single elements) with critical dimensions of $r^*(\theta)$ and $l^*(\theta)$ and the cluster axes within the rod have some orientational fluctuation with respect to the rod axis. Let consider that the rod is formed by the assembly of N aggregates of clusters along the rod axis and M aggregates on the cross section of rod. Thus, the rod length L and the cross section area πR^2 can be approximately represented as Nl^* and $M\pi r^{*2}$, respectively. In this case, we assume that the numbers N and M within a rod are constant, independent of the polar

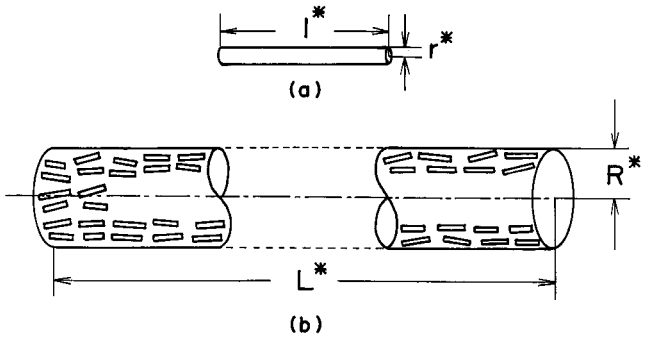

Figure 9. Rod given as an aggregation of a number of single elements with critical dimensions of r^* and l^* with some orientation fluctuation.

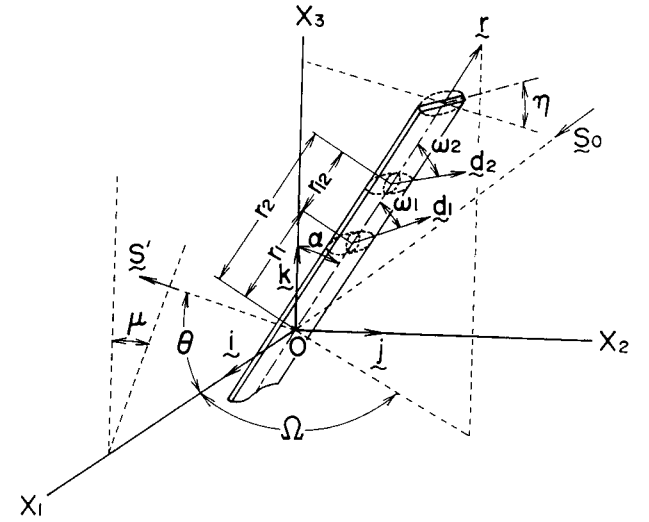

Figure 10. Schematic diagram showing the coordinate system of light scattering from the three-dimensional assembly of anisotropic rod with some orientation fluctuation of the optical axes.

angle θ but the dimension of the rod depends on the cluster size given as a function of θ as described in eqs 49 and 50. Of course, it is evident that the numbers of N satisfy to form a rod whose length is much longer than the wavelength of He−Ne gas laser. This model system represents that, in either folded or fringed type crystal, the optical axes (the c-axes) can be assumed to be oriented parallel to the cluster axis.

According to Rayleigh−Gans theory, the amplitude of the light scattering from a rod may be given by[29]

$$E = C \int \rho_0 \exp[-2\pi i(\mathrm{s}-\mathrm{r_j})]\, \mathrm{d}r \qquad (52)$$

where C is a constant and s is the scattering vector defined by $(s_o - s')/\lambda'$ and λ' is the wavelength of light in the medium. r_0 is the scattering power per unit volume under H_v polarization condition. Figure 9 shows the schematic diagram for calculating the scattered intensity from a rod with the length L and radius R. For simplicity, the calculation at a draw ratio of λ was carried out by putting the rod length L to be $Nl^*(\theta)$, and the rod radius R to be infinitesimally thin. The notation θ in Figure 1a for the polar angle replaces α in Figure 10, since the scattering angle has been represented as θ customarily. The unit vectors s_o and s' are parallel to the propagation direction of the incident and scattered beam, respectively, and θ and μ are the scattering angle and the azimuthal angle, respectively, taken from the vertical direction OX_3 corresponding to a machine (stretching) direction.

In the present model system shown in Figure 9, the orientation of clusters has somewhat fluctuation with respect to the rod axis, while the optical axes have the perfect orientation parallel to the cluster axis. In this case, the orientational fluctuation of the optical axes with respect to the rod axis is equivalent to that of cluster axes with respect to the rod axis. On the basis of this concept, the simple model shown in Figure 10 is proposed, in which the orientation of the optical axes with respect to the rod axis is dependent upon the position within the rod. If the orientation of the optical axis of the scattering element fluctuates around their average value w_0, ω is a function of r like $\omega(r) = w_0 + \Delta(r)$, where $\Delta(r)$ is the local fluctuation of ω. In this viewpoint, the angle w_1 at r_1 and w_2 at r_2 may be given by $w_1 = w_0 + \Delta_1$ and $w_2 = w_0 + \Delta_2$, respectively. When the difference between orientation fluctuation Δ_1 at r_1 and Δ_2 at r_2 is given by Δ_{12}, the quantity Δ_{12} is defined by $\Delta_{12} = \Delta_2 - \Delta_1 = w_2 - w_1$; the angles w_1 and w_2 characterizing the relative orientation of the optical axes of two scattering elements are separated by a distance, $r_{12} = r_1 - r_2$. In the present system, w_0 becomes zero. The quantity Δ_{12} is related to the correlation function $f(r_{12})$,[30] which is given by

$$f(r_{12}) = \langle \cos 2\Delta_{12} \rangle_{\mathrm{av}} \qquad (53)$$

This correlation function is expected to decrease from unity to zero with increasing distance $|r_{12}|$, and is represented by the empirical function

$$f(r_{12}) = \exp\left\{\frac{-|r_{12}|}{c}\right\} \qquad (54)$$

where c is the correlation distance. This empirical function was first introduced to analyze the orientational fluctuations of the optical axes within a spherulite by Stein and Chu.[30] This method is applied to the orientational fluctuation of an optical axis with respect to a rod axis. Thus, $\langle \cos 2\Delta_{12} \rangle_{\mathrm{av}}$ and $\langle \cos^2 2\ \Delta_{12} \rangle_{\mathrm{av}}$ are given by[30−33]

$$\langle \cos 2\Delta_1 \rangle_{\mathrm{av}} = \frac{2}{(L/c)^2}\left[\frac{L}{c} - 1 + \exp\left(-\frac{L}{c}\right)\right] \qquad (55)$$

$$\langle \cos^2 2\Delta_1 \rangle_{\mathrm{av}} = \frac{1}{2} - \frac{1}{16(L/c)^2}\left[1 - 4\frac{L}{c} - \exp\left(-4\frac{L}{c}\right)\right] \qquad (56)$$

where L corresponds to the length $Nl^*(\theta)$ in the undeformed state ($\lambda = 1$).

Equation 55 approaches zero as c approaches zero and approaches unity as c becomes large. On the other hand, eq 56 is $^1/_2$ for a completely random fluctuation corresponding to $c = 0$, and it approaches unity in the absence of internal disorder corresponding to large c. By introducing the orientational fluctuation, the scattered intensity can be written as follows:

$$I_{\mathrm{H_v}} = C' \int_0^{2\pi} \int_0^{\pi} W_{\mathrm{c}}(\alpha) \langle Q \rangle_\eta \sin^2\{bL(\alpha)\} \sin\alpha\, \mathrm{d}\alpha\, \mathrm{d}\Omega \qquad (57)$$

where $W_c(\alpha)$ is the orientational fluctuation of a cluster equivalent to eq 40 and $L(\alpha)$ is given as $Nl^*(\alpha)$ at a draw ratio of λ. From the geometrical arrangement in Figure 10, b is given by

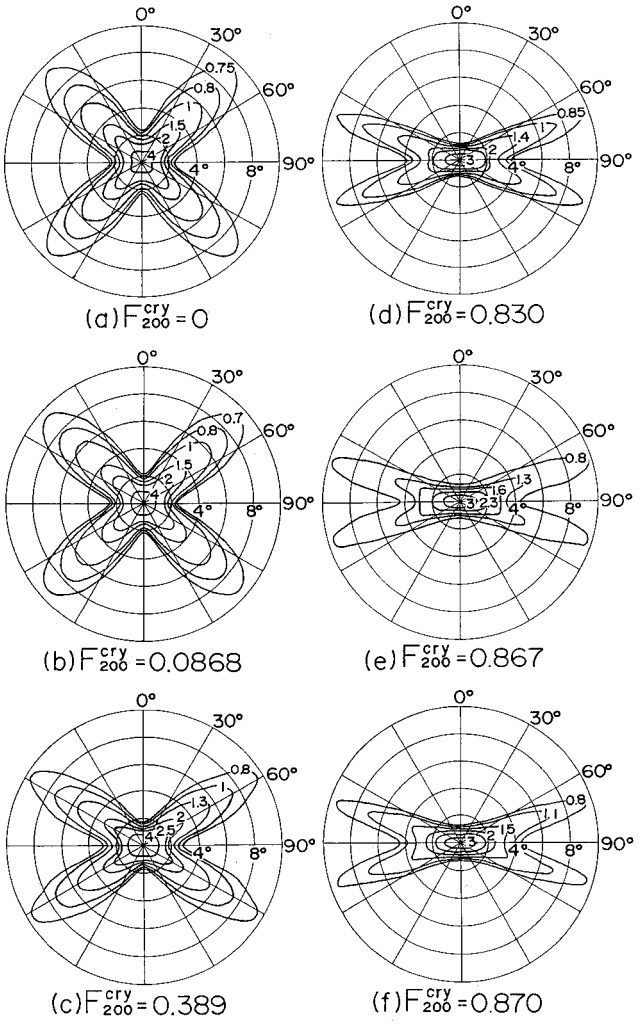

Figure 11. H_v light-scattering patterns calculated without introducing the effect of orientational disorder.

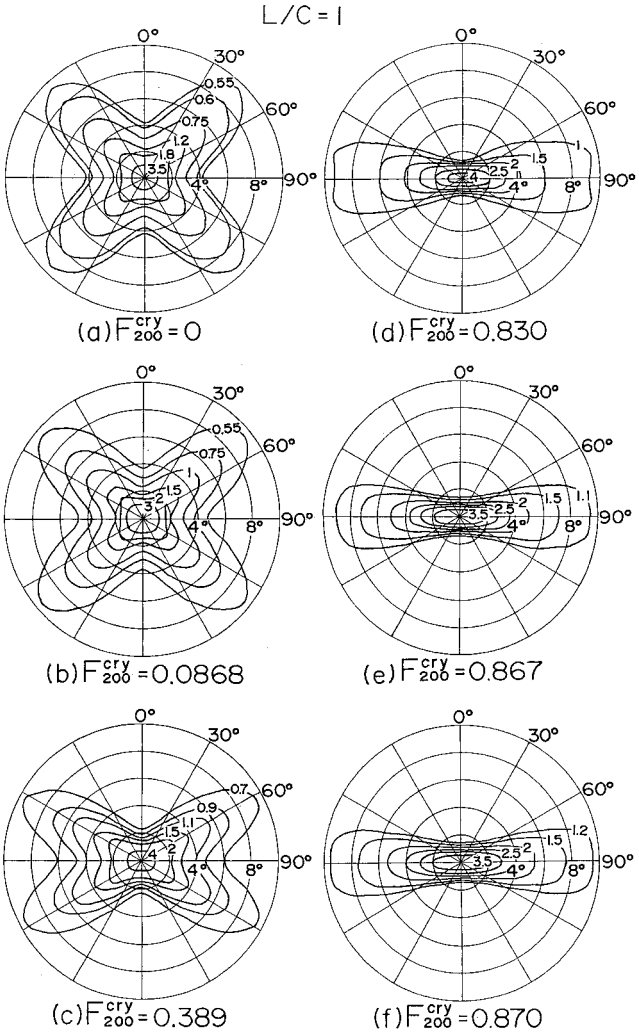

Figure 12. H_v light-scattering patterns calculated by introducing the effect of orientational disorder given as $L/c = 1$.

$$b = \frac{2\pi}{\lambda}\sin\frac{\theta}{2}\left(\sin\frac{\theta}{2}\sin\alpha\cos\Omega - \cos\frac{\theta}{2}\sin\mu\sin\alpha\sin\Omega - \cos\frac{\theta}{2}\cos\mu\cos\alpha\right) \quad (58)$$

and

$$\langle Q\rangle_\eta = \frac{1}{8}\{Q_1\sin^2\alpha\cos^2\alpha\sin^2\Omega + 4Q_2(\cos^2\alpha\cos^2\Omega + \sin^2\Omega) + Q_3\sin^2\alpha\cos^2\Omega\} \quad (59)$$

Here $\langle Q\rangle_\eta$ means the average value found by integrating over the angle η, and the Q_i ($_i = 1-3$) in eq 59 at $w_0 = 0$ are given by

$$Q_1 = \frac{1}{4}[\{35\langle\cos^2 2\Delta_1\rangle_{av} + 5\langle\cos 2\Delta_1\rangle_{av} - 16\}f(r_{12}) + 5\langle\cos 2\Delta_1\rangle_{av} + 3] \quad (60)$$

$$Q_2 = -\frac{1}{4}(\langle\cos^2 2\Delta_1\rangle_{av} - 1)f(r_{12}) \quad (61)$$

$$Q_3 = \frac{1}{4}\{(\langle\cos^2 2\Delta_1\rangle_{av} - \langle\cos 2\Delta_1\rangle_{av})f(r_{12}) - \langle\cos 2\Delta_1\rangle_{av} + 1\} \quad (62)$$

In the numerical calculations below, the scattered intensity was normalized by L^2 in the undrawn state ($\lambda = 1$).

Figures 11 and 12 show light-scattering patterns calculated using the second-order orientation factor F_{200}^{cry} at $L/\lambda' = 40$. The numerical calculations shown in Figure 11 were carried out without introducing the parameter L/c for the orientational disorder of optical axes. These results correspond to the scattering from a system where the optical axes are oriented parallel to the rod axis. The scattered intensity displays an X-type pattern showing a clear μ dependence. Upon increasing the orientation factor, the scattering lobes extend in the horizontal direction, indicating a preferential orientation of the rods with respect to the machine (stretching) direction. Here, it is noted that the change in the patterns is similar to the profile obtained with an affine deformation mode.[34] Also such pattern changes have been usually observed in the course of drawing melt films which contain rods, where the optical axes become oriented parallel or perpendicular to the rod axis.[29] Apart from the patterns in Figures 8 and 11, it has been sometimes observed for calender films that the scattering lobes at the initial elongation stages are extended in the equatorial direction indicating oriented-induced crystallization.[35,36] Such an effect, however, was never observed in the present study, experimentally or theoretically. The theoretical patterns are also in good agreement with the observed patterns.

The patterns in Figure 12 result from the introduction of orientational disorder, i.e., $L/c = 1$. The lobes of the

calculated patterns are broader than the lobes in Figure 11which were calculated without orientational disorder. Further numerical calculations with different values of L/c show that (provided the μ dependence of the scattered intensity distribution becomes more indistinct with increasing orientational fluctuation) the pattern becomes circular at $L/c > 10$. Comparison of the observed pattern in Figure 8 with the calculated patterns in Figures 11 and 12 indicates that the orientational disorder of the optical axes with respect to the rod axis is very small. This suggests that most single elements within a rod orient parallel to the rod axis.

Summary

Three main results are found.

First, the mathematical description of segmental orientation in uniaxially deformed networks was extended past the second order results previously obtained by Erman et al. up to the eighth order. The general approach is based on the methods of Nagai and Flory, and we adopted their nonperturbation treatment of a freely jointed chain. The theory was extended to deformed system by assuming an affine deformation of a free jointed chain. The orientational distribution function is represented as a series of Legendre polynomials containing orientation factors up to the eighth moment. For the same number of freely jointed statistical segments, the second order orientation factor calculated using the results in this paper is almost equal to that calculated by Erman et al., who used a Monte Carlo method. The value of the second order orientation factor eventually becomes larger than one as the number of jointed statistical segments decreases, as has been previously reported by Erman et al. This unsatisfactory behavior is attributed to an approximation which cannot easily be avoided at the present time (See eq 26 in this paper and also see eq 8 in ref 12). However, the problem may be eliminated by selecting an appropriate number of jointed statistical segments for draw ratios < 2.5.

Second, the orientational distribution function of an individual chain element was related to the orientational distribution function of a crystal chain axis using a kinetic theory of nucleation and assuming that orientation of the crystal chain axes is controlled by the distribution of clusters at the saddle point corresponding to nonuniform orientation distribution of steady-state nucleation rates. With this assumption, one assumes that the critical nuclei after formation retain their original orientation in subsequent growth. This kinetic theory was applied to the analysis of the deformation of polyethylene calender films. The orientation functions $2\pi q_j$ (cos θ_j) calculated with this model are in good agreement with the results measured by X-ray diffraction, indicating that the preferential orientation of the *a*-axes with respect to the machine (extruded) direction is due to the rotation of crystallites around their *c*-axis during the extrusion of the melt.

Third, as another application of the model, small-angle light-scattering patterns for H_v polarization were estimated assuming that a rod is formed by aggregation of clusters having the critical sizes. The scattering lobes in the pattern could be extended in the horizontal direction by increasing the orientational order of the rods. The patterns calculated were in good agreement with the ones observed.

Acknowledgment. M.M. wishes to express his hearty thanks to Professors Erman and Bahar of Bogazici University of Turkey for valuable suggestions, when he visited their laboratory.

Appendix 1

The coefficients F_0, F_2, F_4, F_6, and F_8 in eqs 11−14 are given by

$$F_0 = \frac{\sin qr}{qr}$$

$$F_2 = \frac{2\sin qr}{3qr} + 2\frac{\cos qr}{(qr)^2} - 2\frac{\sin qr}{(qr)^3}$$

$$F_4 = \frac{8\sin qr}{35qr} + \frac{16\cos qr}{7(qr)^2} - \frac{72\sin qr}{7(qr)^3} - 24\frac{\cos qr}{(qr)^4} + 24\frac{\sin qr}{(qr)^5}$$

$$F_6 = \frac{16\sin qr}{231qr} + \frac{16\cos qr}{11(qr)^2} - \frac{160\sin qr}{11(qr)^3} - \frac{960\cos qr}{11(qr)^4} + \frac{3600\sin qr}{11(qr)^5} + 720\frac{\cos qr}{(qr)^6} - 720\frac{\sin qr}{(qr)^7}$$

$$F_8 = \frac{128\sin qr}{6435qr} + \frac{512\cos qr}{715(qr)^2} - \frac{1792\sin qr}{143(qr)^3} - \frac{1792\cos qr}{13(qr)^4} + \frac{13440\sin qr}{13(qr)^5} + 5376\frac{\cos qr}{(qr)^6} - 18816\frac{\sin qr}{(qr)^7} - 40320\frac{\cos qr}{(qr)^8} + 40320\frac{\sin qr}{(qr)^9}$$

The terms K_i ($i = 0$ to 8 in eqs 15−18) are expressed in a power series of q as follows:

$$K_0 = 1 + \left(\frac{\langle r^2\rangle_0}{3}\right)^2 g_4 q^4 + \left(\frac{\langle r^2\rangle_0}{3}\right)^3 g_6 q^6 + \left(\frac{\langle r^2\rangle_0}{3}\right)^4 g_8 q^8 + \left(\frac{\langle r^2\rangle_0}{3}\right)^5 g_{10} q^{10} + \left(\frac{\langle r^2\rangle_0}{3}\right)^6 g_{12} q^{12} + \left(\frac{\langle r^2\rangle_0}{3}\right)^7 g_{14} q^{14} + \left(\frac{\langle r^2\rangle_0}{3}\right)^8 g_{16} q^{16}$$

$$K_2 = \left(\frac{\langle r^2\rangle_0}{3}\right)\eta_2 + \left(\frac{\langle r^2\rangle_0}{3}\right)^2 \eta_4 q^2 + \left(\frac{\langle r^2\rangle_0}{3}\right)^3 \eta_6 q^4 + \left(\frac{\langle r^2\rangle_0}{3}\right)^4 \eta_8 q^6 + \left(\frac{\langle r^2\rangle_0}{3}\right)^5 \eta_{10} q^8 + \left(\frac{\langle r^2\rangle_0}{3}\right)^6 \eta_{12} q^{10} + \left(\frac{\langle r^2\rangle_0}{3}\right)^7 \eta_{14} q^{12} + \left(\frac{\langle r^2\rangle_0}{3}\right)^8 \eta_{16} q^{14}$$

$$K_4 = \left(\frac{\langle r^2\rangle_0}{3}\right)^2 z_2 + \left(\frac{\langle r^2\rangle_0}{3}\right)^3 z_4 q^2 + \left(\frac{\langle r^2\rangle_0}{3}\right)^4 z_6 q^4 + \left(\frac{\langle r^2\rangle_0}{3}\right)^5 z_8 q^6$$

$$K_6 = \left(\frac{\langle r^2\rangle_0}{3}\right)^3 s_2 + \left(\frac{\langle r^2\rangle_0}{3}\right)^4 s_4 q^2 + \left(\frac{\langle r^2\rangle_0}{3}\right)^5 s_6 q^4$$

$$K_8 = \left(\frac{\langle r^2\rangle_0}{3}\right)^4 t_2 + \left(\frac{\langle r^2\rangle_0}{3}\right)^5 t_4 q^2$$

The coefficients L_2, L_4, L_6, and L_8 in eqs 15−18 are given as follows:

$$L_2 = \frac{1}{2}(3q_3^2 - q^2)$$

$$L_4 = \frac{1}{8}(35q_3^4 - 30q^2q_3^2 + 3q^4)$$

$$L_6 = \frac{1}{16}(231q_3^6 - 315q^2q_3^4 + 105q^4q_3^2 - 5q^6)$$

$$L_8 = \frac{1}{128}(6435q_3^8 - 12012q^2q_3^6 + 6930q^4q_3^4 - 1260q^6q_3^2 + 35q^8)$$

where $q_3 = q \cos \tau$.

The coefficients g_i ($i = 4$, 6, 8 and 10), η_i ($i = 2$, 4, 6, 8 and 10), Z_i ($i = 2$, 4, 6, and 8), s_i ($i = 2$, 4, and 6), and t_i ($i = 2$ and 4) in eqs 21 and 22 are given by

$$g_4 = -\frac{1}{8} + \frac{3\langle r^4\rangle_0}{40\langle r^2\rangle_0^2}$$

$$g_6 = -\frac{1}{24} - \frac{3\langle r^6\rangle_0}{560\langle r^2\rangle_0^3} + \frac{3\langle r^4\rangle_0}{80\langle r^2\rangle_0^2}$$

$$g_8 = -\frac{1}{128} + \frac{\langle r^8\rangle_0}{4480\langle r^2\rangle_0^4} - \frac{3\langle r^6\rangle_0}{1120\langle r^2\rangle_0^3} + \frac{3\langle r^4\rangle_0}{320\langle r_2^2\rangle_0^2}$$

$$g_{10} = -\frac{1}{960} - \frac{3\langle r^{10}\rangle_0}{492800\langle r^2\rangle_0^5} + \frac{\langle r^8\rangle_0}{8960\langle r^2\rangle_0^4} - \frac{3\langle r^6\rangle_0}{4480\langle r^2\rangle_0^3} + \frac{\langle r^4\rangle_0}{640\langle r^2\rangle_0^2}$$

$$g_{12} = -\frac{1}{9216} + \frac{3\langle r^{12}\rangle_0}{25625600\langle r^2\rangle_0^6} - \frac{3\langle r^{10}\rangle_0}{985600\langle r^2\rangle_0^5} + \frac{\langle r^8\rangle_0}{35840\langle r^2\rangle_0^4} - \frac{\langle r^6\rangle_0}{8960\langle r^2\rangle_0^3} + \frac{\langle r^4\rangle_0}{5120\langle r^2\rangle_0^2}$$

$$g_{14} = -\frac{1}{107520} - \frac{3\langle r^{14}\rangle_0}{1793792000\langle r^2\rangle_0^7} + \frac{3\langle r^{12}\rangle_0}{51251200\langle r^2\rangle_0^6} - \frac{3\langle r^{10}\rangle_0}{3942400\langle r^2\rangle_0^5} + \frac{\langle r^8\rangle_0}{215040\langle r^2\rangle_0^4} - \frac{\langle r^6\rangle_0}{71680\langle r^2\rangle_0^3} + \frac{\langle r^4\rangle_0}{51200\langle r^2\rangle_0^2}$$

$$g_{16} = -\frac{1}{1474560} + \frac{9\langle r^{16}\rangle_0}{487911424000\langle r^2\rangle_0^8} - \frac{3\langle r^{14}\rangle_0}{3587584000\langle r^2\rangle_0^7} + \frac{3\langle r^{12}\rangle_0}{205004800\langle r^2\rangle_0^6} - \frac{\langle r^{10}\rangle_0}{7884800\langle r^2\rangle_0^5} + \frac{\langle r^8\rangle_0}{1720320\langle r^2\rangle_0^4} - \frac{\langle r^6\rangle_0}{716800\langle r^2\rangle_0^3} + \frac{\langle r^4\rangle_0}{614400\langle r^2\rangle_0^2}$$

$$\eta_2 = -\frac{2\langle r^2 P_2(\cos\Phi)\rangle_0}{15\langle r^2\rangle_0}$$

$$\eta_4 = \frac{\langle r^4 P_2(\cos\Phi)\rangle_0}{35\langle r^2\rangle_0^2} - \frac{\langle r^2 P_2(\cos\Phi)\rangle_0}{15\langle r^2\rangle_0}$$

$$\eta_6 = -\frac{\langle r^6 P_2(\cos\Phi)\rangle_0}{420\langle r^2\rangle_0^3} + \frac{\langle r^4 P_2(\cos\Phi)\rangle_0}{70\langle r^2\rangle_0^2} - \frac{\langle r^2 P_2(\cos\Phi)\rangle_0}{60\langle r^2\rangle_0}$$

$$\eta_8 = \frac{\langle r^8 P_2(\cos\Phi)\rangle_0}{9240\langle r^2\rangle_0^4} - \frac{\langle r^6 P_2(\cos\Phi)\rangle_0}{840\langle r^2\rangle_0^3} + \frac{\langle r^4 P_2(\cos\Phi)\rangle_0}{280\langle r^2\rangle_0^2} - \frac{\langle r^2 P_2(\cos\Phi)\rangle_0}{360\langle r^2\rangle_0}$$

$$\eta_{10} = -\frac{\langle r^{10} P_2(\cos\Phi)\rangle_0}{320320\langle r^2\rangle_0^5} + \frac{\langle r^8 P_2(\cos\Phi)\rangle_0}{18480\langle r^2\rangle_0^4} - \frac{\langle r^6 P_2(\cos\Phi)\rangle_0}{3360\langle r^2\rangle_0^3} + \frac{\langle r^4 P_2(\cos\Phi)\rangle_0}{1680\langle r^2\rangle_0^2} - \frac{\langle r^2 P_2(\cos\Phi)\rangle_0}{2880\langle r^2\rangle_0}$$

$$\eta_{12} = \frac{\langle r^{12} P_2(\cos\Phi)\rangle_0}{16016000\langle r^2\rangle_0^6} - \frac{\langle r^{10} P_2(\cos\Phi)\rangle_0}{640640\langle r^2\rangle_0^5} + \frac{\langle r^8 P_2(\cos\Phi)\rangle_0}{73920\langle r^2\rangle_0^4} - \frac{\langle r^6 P_2(\cos\Phi)\rangle_0}{20160\langle r^2\rangle_0^3} + \frac{\langle r^4 P_2(\cos\Phi)\rangle_0}{13440\langle r^2\rangle_0^2} - \frac{\langle r^2 P_2(\cos\Phi)\rangle_0}{28800\langle r^2\rangle_0^2}$$

$$\eta_{14} = -\frac{\langle r^{14} P_2(\cos\Phi)\rangle_0}{1089088000\langle r^2\rangle_0^7} + \frac{\langle r^{12} P_2(\cos\Phi)\rangle_0}{32032000\langle r^2\rangle_0^6} - \frac{\langle r^{10} P_2(\cos\Phi)\rangle_0}{2562560\langle r^2\rangle_0^5} + \frac{\langle r^8 P_2(\cos\Phi)\rangle_0}{443520\langle r^2\rangle_0^4} - \frac{\langle r^6 P_2(\cos\Phi)\rangle_0}{161280\langle r^2\rangle_0^3} + \frac{\langle r^4 P_2(\cos\Phi)\rangle_0}{134400\langle r^2\rangle_0^2} - \frac{\langle r^2 P_2(\cos\Phi)\rangle_0}{345600\langle r^2\rangle_0}$$

$$\eta_{16} = \frac{3\langle r^{16} P_2(\cos\Phi)\rangle_0}{289697408000\langle r^2\rangle_0^8} - \frac{\langle r^{14} P_2(\cos\Phi)\rangle_0}{2178176000\langle r^2\rangle_0^7} + \frac{\langle r^{12} P_2(\cos\Phi)\rangle_0}{128128000\langle r^2\rangle_0^6} - \frac{\langle r^{10} P_2(\cos\Phi)\rangle_0}{15375360\langle r^2\rangle_0^5} + \frac{\langle r^8 P_2(\cos\Phi)\rangle_0}{3548160\langle r^2\rangle_0^4} - \frac{\langle r^6 P_2(\cos\Phi)\rangle_0}{1612800\langle r^2\rangle_0^3} + \frac{\langle r^4 P_2(\cos\Phi)\rangle_0}{1612800\langle r^2\rangle_0^2} - \frac{\langle r^2 P_2(\cos\Phi)\rangle_0}{4838400\langle r^2\rangle_0}$$

$$z_2 = \frac{8\langle r^4 P_4(\cos\Phi)\rangle_0}{3675\langle r^2\rangle_0^2}$$

$$z_4 = -\frac{4\langle r^6 P_4(\cos\Phi)\rangle_0}{13475\langle r^2\rangle_0^3} + \frac{4\langle r^4 P_4(\cos\Phi)\rangle_0}{3675\langle r^2\rangle_0^2}$$

$$z_6 = \frac{3\langle r^8 P_4(\cos\Phi)\rangle_0}{175175\langle r^2\rangle_0^4} - \frac{2\langle r^6 P_4(\cos\Phi)\rangle_0}{13475\langle r^2\rangle_0^3} + \frac{\langle r^4 P_4(\cos\Phi)\rangle_0}{3675\langle r^2\rangle_0^2}$$

$$z_8 = -\frac{\langle r^{10} P_4(\cos\Phi)\rangle_0}{1751750\langle r^2\rangle_0^5} + \frac{3\langle r^8 P_4(\cos\Phi)\rangle_0}{350350\langle r^2\rangle_0^4} - \frac{\langle r^6 P_4(\cos\Phi)\rangle_0}{26950\langle r^2\rangle_0^3} + \frac{\langle r^4 P_4(\cos\Phi)\rangle_0}{22050\langle r^2\rangle_0^2}$$

$$s_2 = -\frac{16\langle r^6 P_6(\cos\Phi)\rangle_0}{1156155\langle r^2\rangle_0^3}$$

$$s_4 = \frac{8\langle r^8 P_6(\cos\Phi)\rangle_0}{5780775\langle r^2\rangle_0^4} - \frac{8\langle r^6 P_6(\cos\Phi)\rangle_0}{1156155\langle r^2\rangle_0^3}$$

$$s_6 = -\frac{2\langle r^{10} P_6(\cos\Phi)\rangle_0}{32757725\langle r^2\rangle_0^5} + \frac{4\langle r^8 P_6(\cos\Phi)\rangle_0}{5780775\langle r^2\rangle_0^4} - \frac{2\langle r^6 P_6(\cos\Phi)\rangle_0}{1156155\langle r^2\rangle_0^3}$$

$$t_2 = \frac{128\langle r^8 P_8(\cos\Phi)\rangle_0}{2737609875\langle r^2\rangle_0^4}$$

$$t_4 = -\frac{64\langle r^{10} P_8(\cos\Phi)\rangle_0}{17338195875\langle r^2\rangle_0^5} + \frac{64\langle r^8 P_8(\cos\Phi)\rangle_0}{2737609875\langle r^2\rangle_0^4}$$

Appendix 2

G_i ($i = 4-10$) in eq 21, Y_i ($i = 2-10$) in eq 22, Z_i ($i = 2-8$) in eq 23, S_i ($i = 2-6$) in eq 24 and T_i ($i = 2-4$) in eq 25 are given by

$$G_4 = \frac{3(3r^4 - 10r^2\langle r^2\rangle_0 + 5\langle r^2\rangle_0^2)}{\langle r^2\rangle_0^2}$$

$$G_6 = \frac{3(-9r^6 + 63r^4\langle r^2\rangle_0 - 105r^2\langle r^2\rangle_0^2 + 35\langle r^2\rangle_0^3)}{\langle r^2\rangle_0^3}$$

$$G_8 = [27(3r^8 - 36r^6\langle r^2\rangle_0 + 126r^4\langle r^2\rangle_0^2 - 140r^2\langle r^2\rangle_0^3 + 35\langle r^2\rangle_0^4)]/[\langle r^2\rangle_0^4]$$

$$G_{10} = 27(-9r^{10} + 165r^8\langle r^2\rangle_0 - 990r^6\langle r^2\rangle_0^2 + 2310r^4\langle r^2\rangle_0^3 - 1925r^2\langle r^2\rangle_0^4 + 385\langle r^2\rangle_0^5)/\langle r^2\rangle_0^5$$

$$G_{12} = 27(27r^{12} - 702r^{10}\langle r^2\rangle_0 + 6435r^8\langle r^2\rangle_0^2 - 25740r^6\langle r^2\rangle_0^3 + 45045r^4\langle r^2\rangle_0^4 - 30030r^2\langle r^2\rangle_0^5 + 5005\langle r^2\rangle_0^6)/\langle r^2\rangle_0^6$$

$$G_{14} = 81(-27r^{14} + 945r^{12}\langle r^2\rangle_0 - 12285r^{10}\langle r^2\rangle_0^2 + 75075r^8\langle r^2\rangle_0^3 - 225225r^6\langle r^2\rangle_0^4 + 315315r^4\langle r^2\rangle_0^5 - 175175r^2\langle r^2\rangle_0^6 + 25025\langle r^2\rangle_0^7)/\langle r^2\rangle_0^7$$

$$G_{16} = 81(81r^{16} - 3672r^{14}\langle r^2\rangle_0 + 64260r^{12}\langle r^2\rangle_0^2 - 556920r^{10}\langle r^2\rangle_0^3 + 2552550r^8\langle r^2\rangle_0^4 - 6126120r^6\langle r^2\rangle_0^5 + 7147140r^4\langle r^2\rangle_0^6 - 3403400r^2\langle r^2\rangle_0^7 + 425425\langle r^2\rangle_0^8)/\langle r^2\rangle_0^8$$

$$Y_2 = \frac{3C_2^{(n)}(r^2 - 3x^2)}{2C_0^{(n)}\langle r^2\rangle_0}$$

$$Y_4 = \frac{3C_2^{(n)}(-3r^2 + 7\langle r^2\rangle_0)(r^2 - 3x^2)}{2C_0^{(n)}\langle r^2\rangle_0^2}$$

$$Y_6 = \frac{27C_2^{(n)}(r^4 - 6r^2\langle r^2\rangle_0 + 7\langle r^2\rangle_0^2)(r^2 - 3x^2)}{2C_0^{(n)}\langle r^2\rangle_0^3}$$

$$Y_8 = 27C_2^{(n)}(-3r^6 + 33r^4\langle r^2\rangle_0 - 99r^2\langle r^2\rangle_0^2 + 77\langle r^2\rangle_0^3)(r^2 - 3x^2)/(2C_0^{(n)}\langle r^2\rangle_0^4)$$

$$Y_{10} = 27C_2^{(n)}(9r^8 - 156r^6\langle r^2\rangle_0 + 858r^4\langle r^2\rangle_0^2 - 1716r^2\langle r^2\rangle_0^3 + 1001\langle r^2\rangle_0^4)(r^2 - 3x^2)/(2C_0^{(n)}\langle r^2\rangle_0^5)$$

$$Y_{12} = 81C_2^{(n)}(-9r^{10} + 225r^8\langle r^2\rangle_0 - 1950r^6\langle r^2\rangle_0^2 + 7150r^4\langle r^2\rangle_0^3 - 10725r^2\langle r^2\rangle_0^4 + 5005\langle r^2\rangle_0^5)(r^2 - 3x^2)/(2C_0^{(n)}\langle r^2\rangle_0^6)$$

$$Y_{14} = 81C_2^{(n)}(27r^{12} - 918r^{10}\langle r^2\rangle_0 + 11475r^8\langle r^2\rangle_0^2 - 66300r^6\langle r^2\rangle_0^3 + 182325r^4\langle r^2\rangle_0^4 - 218790r^2\langle r^2\rangle_0^5 + 85085\langle r^2\rangle_0^6)(r^2 - 3x^2)/(2C_0^{(n)}\langle r^2\rangle_0^7)$$

$$Y_{16} = 81C_2^{(n)}(-81r^{14} + 3591r^{12}\langle r^2\rangle_0 - 61047r^{10}\langle r^2\rangle_0^2 + 508725r^8\langle r^2\rangle_0^3 - 2204475r^6\langle r^2\rangle_0^4 + 4849845r^4\langle r^2\rangle_0^5 - 4849845r^2\langle r^2\rangle_0^6 + 1616615\langle r^2\rangle_0^7)(r^2 - 3x^2)/(2C_0^{(n)}\langle r^2\rangle_0^8)$$

$$Z_2 = \frac{9C_4^{(n)}(3r^4 - 30r^2x^2 + 35x^4)}{8C_0^{(n)}\langle r^2\rangle_0^2}$$

$$Z_4 = \frac{9C_4^{(n)}(-3r^2 + 11\langle r^2\rangle_0)(3r^4 - 30r^2x^2 + 35x^4)}{8C_0^{(n)}\langle r^2\rangle_0^3}$$

$$Z_6 = \frac{9C_4^{(n)}(9r^4 - 78r^2\langle r^2\rangle_0 + 143\langle r^2\rangle_0^2)(3r^4 - 30r^2x^2 + 35x^4)}{8C_0^{(n)}\langle r^2\rangle_0^4}$$

$$Z_8 = [27C_4^{(n)}(-9r^6 + 135r^4\langle r^2\rangle_0 - 585\langle r^2\rangle_0^2 + 715\langle r^2\rangle_0^3)(3r^4 - 30r^2x^2 + 35x^4)]/[8C_0^{(n)}\langle r^2\rangle_0^5]$$

$$S_2 = \frac{27C_6^{(n)}(5r^6 - 105r^4x^2 + 315r^2x^4 - 231x^6)}{16C_0^{(n)}\langle r^2\rangle_0^3}$$

$$S_4 = [81C_6^{(n)}(r^2 - 5\langle r^2\rangle_0)(-5r^6 + 105r^4x^2 - 315r^2x^4 + 231x^6)]/[16C_0^{(n)}\langle r^2\rangle_0^4]$$

$$S_6 = [81C_6^{(n)}(-3r^4 + 34r^2\langle r^2\rangle_0 - 85\langle r^2\rangle_0^2)(-5r^6 + 105r^4x^2 - 315r^2x^4 + 231x^6)]/[16C_0^{(n)}\langle r^2\rangle_0^5]$$

$$T_2 = [81C_8^{(n)}(35r^8 - 1260r^6x^2 + 6930r^4x^4 - 12012r^2x^6 + 6435x^8)]/[128C_0^{(n)}\langle r^2\rangle_0^4]$$

$$T_4 = [81C_8^{(n)}(-3r^2 + 19\langle r^2\rangle_0)(35r^8 - 1260r^6x^2 + 6930r^4x^4 - 12012r^2x^6 + 6435x^8)]/[128C_0^{(n)}\langle r^2\rangle_0^5]$$

where $r^2 = x^2 + y^2 + z^2$.

Appendix 3

The coefficient D_i ($i = 4-10$), E_i ($i = 2-4$), F_i ($i = 3, 4$) and H_4 in eq 44 are given by

$$D_1 = C_2^{(n)}(-1 + 10395g_{10} + 135135g_{12} + 2027025g_{14} + 34459425g_{16} + 15g_4 + 105g_6 + 945g_8)(9009\eta_{10} + 135135\eta_{12} + 2297295\eta_{14} + 43648605\eta_{16} + \eta_2 + 7\eta_4 + 63\eta_6 + 693\eta_8)/C_0^{(n)}$$

$$D_2 = 9C_2^{(n)}\frac{\langle r^4\rangle_0}{\langle r^2\rangle_0^2}\{5148\eta_{10} - 209594385g_{10}\eta_{10} - 3130537410g_{12}\eta_{10} - 53045217225g_{14}\eta_{10} - 1005250346100g_{16}\eta_{10} - 167310g_4\eta_{10} - 1486485g_6\eta_{10} - 16216200g_8\eta_{10} + 96525\eta_{12} - 3344591250g_{10}\eta_{12} - 49566842325g_{12}\eta_{12} - 834809976000g_{14}\eta_{12} - 15743994391125g_{16}\eta_{12} - 2799225g_4\eta_{12} - 24324300g_6\eta_{12} - 261486225g_8\eta_{12} + 1969110\eta_{14} - 60269534325g_{10}\eta_{14} - 886985599500g_{12}\eta_{14} - 14857008791625g_{14}\eta_{14} - 278956971042750g_{16}\eta_{14} - 52509600g_4\eta_{14} - 447972525g_6\eta_{14} - 4755400650g_8\eta_{14} + 43648605\eta_{16} - 1209939330600g_{10}\eta_{16} - 17695362710025g_{12}\eta_{16} - 294922711833750g_{14}\eta_{16} - 5515054711291125g_{16}\eta_{16} - 1091215125g_4\eta_{16} - 9166207050g_6\eta_{16} - 96245174025g_8\eta_{16} - 17325g_{10}\eta_2 - 270270g_{12}\eta_2 - 4729725g_{14}\eta_2 - 91891800g_{16}\eta_2 - 10g_4\eta_2 - 105g_6\eta_2 - 1260g_8\eta_2 + \eta_4 - 131670g_{10}\eta_4 - 2027025g_{12}\eta_4 - 35135100g_{14}\eta_4 - 677702025g_{16}\eta_4 - 85g_4\eta_4 - 840g_6\eta_4 - 9765g_8\eta_4 + 18\eta_6 - 1278585g_{10}\eta_6 - 19459440g_{12}\eta_6 - 334459125g_{14}\eta_6 - 6409453050g_{16}\eta_6 - 900g_4\eta_6 - 8505g_6\eta_6 - 96390g_8\eta_6 + 297\eta_8 - 15093540g_{10}\eta_8 - 227432205g_{12}\eta_8 - 3879725850g_{14}\eta_8 - 73915466625g_{16}\eta_8 - 11385g_4\eta_8 - 103950g_6\eta_8 - 1153845g_8\eta_8\}/(5C_0^{(n)})$$

$$D_3 = 135C_2^{(n)}\frac{\langle r^6\rangle_0}{\langle r^2\rangle_0^3}\{-858\eta_{10} + 160540380g_{10}\eta_{10} + 2724727005g_{12}\eta_{10} + 51653867265g_{14}\eta_{10} + 1082122431390g_{16}\eta_{10} + 73359g_4\eta_{10} + 819819g_6\eta_{10}''' + 10702692g_8\eta_{10} - 21450\eta_{12} + 2831753925g_{10}\eta_{12} + 47247925725g_{12}\eta_{12} + 883507224600g_{14}\eta_{12} + 18301469536350g_{16}\eta_{12} + 1422135g_4\eta_{12} + 15225210g_6\eta_{12} + 192972780g_8\eta_{12} - 546975\eta_{14} + 55720890225g_{10}\eta_{14} + 916551786150g_{12}\eta_{14} + 16941424950450g_{14}\eta_{14} + 347565307164075g_{16}\eta_{14} + 30193020g_4\eta_{14} + 312432120g_6\eta_{14} + 3866347485g_8\eta_{14} - 14549535\eta_{16} + 1209939330600g_{10}\eta_{16} + 19661514122250g_{12}\eta_{16} + 359805708437175g_{14}\eta_{16} + 7319981707713675g_{16}\eta_{16} + 698377680g_4\eta_{16} + 7027425405g_6\eta_{16} + 85245725565g_8\eta_{16} + 6930g_{10}\eta_2 + 135135g_{12}\eta_2 + 2837835g_{14}\eta_2 + 64324260g_{16}\eta_2 + g_4\eta_2 + 21g_6\eta_2 + 378g_8\eta_2 + 65835g_{10}\eta_4 + 1216215g_{12}\eta_4 + 24594570g_{14}\eta_4 + 542161620g_{16}\eta_4 + 17g_4\eta_4 + 252g_6\eta_4 + 3906g_8\eta_4 - \eta_6 + 758835g_{10}\eta_6 + 13513500g_{12}\eta_6 + 265945680g_{14}\eta_6 + 5740940205g_{16}\eta_6 + 258g_4\eta_6 + 3318g_6\eta_6 + 47439g_8\eta_6 - 33\eta_8 + 10291050g_{10}\eta_8 + 178378200g_{12}\eta_8 + 3438239805g_{14}\eta_8 + 73005737805g_{16}\eta_8 + 4158g_4\eta_8 + 49203g_6\eta_8 + 667359g_8\eta_8\}/35C_0^{(n)}$$

$$D_4 = 315C_2^{(n)}\frac{\langle r^8\rangle_0}{\langle r^2\rangle_0^4}\{52\eta_{10} - 59999940g_{10}\eta_{10} - 1166485320g_{12}\eta_{10} - 24859840005g_{14}\eta_{10} - 577346990220g_{16}\eta_{10} - 14508g_4\eta_{10} - 212667g_6\eta_{10} - 3400488g_8\eta_{10} + 1950\eta_{12} - 1194593400g_{10}\eta_{12} - 22583085525g_{12}\eta_{12} - 470634664500g_{14}\eta_{12} - 10730733863850g_{16}\eta_{12} - 340275g_4\eta_{12} - 4619160g_6\eta_{12} - 70221060g_8\eta_{12} + 66300\eta_{14} - 26085784725g_{10}\eta_{14} - 482018436900g_{12}\eta_{14} - 9861667165350g_{14}\eta_{14} - 221429235327300g_{16}\eta_{14} - 8433360g_4\eta_{14} - 108042480g_6\eta_{14} - 1578868200g_8\eta_{14} + 2204475\eta_{16} - 620683163100g_{10}\eta_{16} - 11252173882950g_{12}\eta_{16} - 226643635518300g_{14}\eta_{16} - 5022801894084975g_{16}\eta_{16} - 222211080g_4\eta_{16} - 2719440360g_6\eta_{16} - 38486165445g_8\eta_{16} - 990g_{10}\eta_2 - 25740g_{12}\eta_2 - 675675g_{14}\eta_2 - 18378360g_{16}\eta_2 - g_6\eta_2 - 36g_8\eta_2 - 13860g_{10}\eta_4 - 315315g_{12}\eta_4 - 7567560g_{14}\eta_4 - 192972780g_{16}\eta_4 - g_4\eta_4 - 28g_6\eta_4 - 630g_8\eta_4 - 204435g_{10}\eta_6 - 4324320g_{12}\eta_6 - 98378280g_{14}\eta_6 - 2407565160g_{16}\eta_6 - 28g_4\eta_6 - 546g_6\eta_6 - 10332g_8\eta_6 + \eta_8 - 3326400g_{10}\eta_8 - 67026960g_{12}\eta_8 - 1469187720g_{14}\eta_8 - 34907397525g_{16}\eta_8 - 642g_4\eta_8 - 10500g_6\eta_8 - 179739g_8\eta_8\}/35C_0^{(n)}$$

$$E_2 = 9C_4^{(n)}\frac{\langle r^4\rangle_0}{\langle r^2\rangle_0^2}(1 - 10395g_{10} - 15g_4 - 105g_6 - 945g_8)(z_2 + 11z_4 + 143z_6 + 2145z_8)/5C_0^{(n)}$$

$$E_3 = 135C_4^{(n)}\frac{\langle r^6\rangle_0}{\langle r^2\rangle_0^3}(17325g_{10}z_2 + 10g_4z_2 + 105g_6z_2 + 1260g_8z_2 - z_4 + 200970g_{10}z_4 + 125g_4z_4 + 1260g_4z_4 + 14805g_6z_4 - 26z_6 + 2747745g_{10}z_6 + 1820g_4z_6 + 17745g_6z_6 + 204750g_8z_6 - 585z_8 + 43243200g_{10}z_8 + 30225g_4z_8 + 286650g_6z_8 + 3255525g_8z_8)/35C_0^{(n)}$$

$$E_4 = 315C_4^{(n)}\frac{\langle r^8\rangle_0}{\langle r^2\rangle_0^4}(-6930g_{10}z_2 - g_4z_2 - 21g_6z_2 - 378g_8z_2 - 93555g_{10}z_4 - 21g_4z_4 - 336g_6z_4 - 5418g_8z_4 + z_6 - 1451835g_{10}z_6 - 418g_4z_6 - 5838g_6z_6 - 87759g_8z_6 + 45z_8 - 25467750g_{10}z_8 - 8670g_4z_8 - 111195g_6z_8 - 1590435g_8z_8)/35C_0^{(n)}$$

$$F_3 = 27C_6^{(n)}\frac{\langle r^6\rangle_0}{\langle r^2\rangle_0^3}(-1 + 10395g_{10} + 15g_4 + 105g_6 + 945g_8)(s_2 + 15s_4 + 255s_6)/7C_0^{(n)}$$

$$F_4 = 63C_6^{(n)}\frac{\langle r^8\rangle_0}{\langle r^2\rangle_0^4}(-17325g_{10}s_2 - 10g_4s_2 - 105g_6s_2 - 1260g_8s_2 + s_4 - 270270g_{10}s_4 - 165g_4s_4 - 1680g_6s_4 - 19845g_8s_4 + 34s_6 - 4771305g_{10}s_6 - 3060g_4s_6 - 30345g_6s_6 - 353430g_8s_6)/7C_0^{(n)}$$

$$H_4 = 9C_8^{(n)}\frac{\langle r^8\rangle_0}{\langle r^2\rangle_0^4}(1 - 10395g_{10} - 15g_4 - 105g_6 - 945g_8)(t_2 - 19t_4)/C_0^{(n)}$$

Note Added After Print Publication

This article was released ASAP on 4/27/2002 and appeared in the May 21, 2002, issue (Vol. 35, No. 11, pp 4493−4509) with errors in eq 26 and the text below it. The correct electronic version was posted on 6/13/2002, and an Addition and Correction appears in the July 16, 2002, issue (Vol. 35, No. 15).

References and Notes

(1) Roe, R. J.; Krigbaum, W. R. *J. Chem. Phys.* **1964**, *40*, 2608.
(2) Krigbaum, W. R.; Roe, R. J.*J. Chem. Phys.* **1964**, *41*, 737.
(3) Roe, R. J.; Krigbaum, W. R. *J. Appl. Phys.* **1964**, *35*, 2215.
(4) Kuhn, W.; Grün, F. *Kolloid-Z.* **1942**, *101*, 248.
(5) Treloar, L. R. *Trans. Faraday Soc.* **1964**, *50*, 881.
(6) DiMarzio, E. A. *J. Chem. Phys.* **1962**, *36*, 1563.
(7) Tanaka, T.; Allen, G. *Macromolecules* **1977**, *10*, 426.
(8) Jarry, J. P.; Monnerie, L. *Macromolecules* **1979**, *12*, 316.
(9) Erman, B.; Bahar, I.; Kloczkowski, A.; Mark, J. E. *Macromolecules* **1990**, *23*, 5335.
(10) Bahar, I.; Erman, B.; Kloczkowski, A.; Mark, J. E. *Macromolecules* **1990**, *23*, 5341.
(11) Matsuo, M.; Ooki, J.; Harashina, Y.; Ogita, T.; Manley, R. S. J. *Macromolecules* **1995**, *28*, 4951.
(12) Erman, B.; Haliloglu, T.; Bahar, I.; Mark, J. E. *Macromolecules* **1991**, *24*, 901.
(13) Nagai, K.*J. Chem. Phys.* **1964**, *40*, 2818.
(14) Flory, P. J. *Statistical Mechanics of Chain Molecules*; Interscience: New York, 1969.
(15) Shimizu, Y.; Harashina, Y.; Sugiura, Y.; Matsuo, M. *Macromolecules* **1995**, *28*, 6889.
(16) Bunn, C. W. *Trans. Faraday Soc.* **1939**, *35*, 482.
(17) Sawatari, C.; Okumura, T.; Matsuo, M. *Polym. J.* **1986**, *18*, 741.
(18) Matsuo, M.; Sawatari, C.; Ohhata, T. *Macromolecules* **1988**, *21*, 1317.
(19) Matsuo, M.; Sawatari, C. *Macromolecules* **1986**, *19*, 2036.
(20) Stein, R. S.; Norris, F. H.*J. Polym. Sci.* **1956**, *21*, 381.
(21) Bunn, C. W.; de Daubeny, R. *Trans. Faraday Soc.* **1954**, *50*, 1173.
(22) Ziabicki, A.; Jarecki, L. *Colloid Polym. Sci.* **1978**, *256*, 332.
(23) Kosc, M.; Ziabicki, A. *Macromolecules* **1982**, *15*, 1507.
(24) Hashimoto, T.; Saijo, K.; Kosc, M.; Kawai, H.; Wasiak, A.; Ziabicki, A. *Macromolecules* **1985**, *18*, 472.
(25) Hoffman, J. D.; Lauritzen, J. I.; Passaglia, E., Jr.; Ross, G. S.; Frolen, L. J.; Weeks, J. J. *Kolloid Z. Z. Polym.* **1969**, *231*, 564.
(26) Mandelkern, L. *Crystallization of Polymer*; McGraw-Hill: New York, 1964.
(27) Hoffman, J. D.; Davies, G. T.; Lauritzen, J. Jr. *Treatise Solid State Chem.* **1976**, 3.
(28) Spendly, W.; Hext, G. R.; Homsworth, F. R. *Technometrics* **1962**, *4*, 441.
(29) Rhodes, M. B.; Stein, R. S. *J. Polym. Sci., Part A-2* **1969**, *7*, 1539.
(30) Stein, R. S.; Chu, W. *J. Polym. Sci. A-2* **1970**, *8*, 1137.
(31) Hashimoto, T.; Murakami, Y.; Hayashi, N.; Kawai, H. *Polym. J.* **1974**, *6*, 132.
(32) Ozaki, F.; Ogita, T.; Matsuo, M. *Macromolecules* **1981**, *14*, 299.
(33) Matsuo, M.; Kakei, K.; Nagaoka, Y.; Ozaki, F.; Murai, M.; Ogita, T. *J. Chem. Phys.* **1981**, *75*, 5911.
(34) Sugiura, Y.; Matsuo, M. Manuscript in preparation.
(35) Hashimoto, T.; Ishido, S.; Kawai, H.; Ziabicki, A. *Macromolecules* **1978**, *11*, 1210.
(36) Sawatari, C.; Iida, M.; Matsuo, M. *Macromolecules* **1984**, *17*, 1765.

MA0007839